The 12th Symposium on Polar Science
15 – 18 November 2021

National Institute of Polar Research
Research Organization of Information and Systems

Session OA
Antarctic meteorites

Program and Abstracts

Convener : Naoya Imae (NIPR)

【OA】Antarctic meteorites

Scopes

This session is held to present recent research outcomes for Antarctic meteorites and micrometeorites. It will also be an opportunity for general and topical discussion sessions dealing with new data from non-Antarctic meteorites and extraterrestrial materials, and related experimental and theoretical works.

Convener : **Naoya Imae (NIPR)**

Real-time Oral presentations (13:10 – 16:15)

Date: Thu. 18 November

Chair: Akira Yamaguchi (NIPR)				
	13:10 - 13:15	Opening	Akira Yamaguchi (NIPR), Naoya Imae (NIPR)	
OAo1	13:15 - 13:30	Lithium, and boron isotopic compositions of chondrule olivine from Yamato 81020, Asuka 12236 and QUE 97008 chondrites	*Nozomi Matsuda (UCLA) and Ming-Chang Liu (UCLA)	OA_Matsuda_00591_01
OAo2	13:30 - 13:45	Tarda: A highly aqueously altered meteorite from an outer Solar System asteroid?	* Devin L. Schrader (Center for Meteorite Studies, School of Earth and Space Exploration, Arizona State University), Jemma Davidson (Center for Meteorite Studies, School of Earth and Space Exploration, Arizona State University), Dionysis Foustoukos (Earth and Planetary Laboratory, Carnegie Institution for Science), Conel M. O'D. Alexander (Earth and Planetary Laboratory, Carnegie Institution for Science) and Thomas J. Zega (Lunar and Planetary Laboratory	OA_Schrader_00141_01
OAo3	13:45 - 14:00	Carbonate minerals in the highly-altered A-12248 CM chondrite	*Kaitlyn A. McCain (University of California at Los Angeles), Ming-Chang Liu (University of California at Los Angeles) and Kevin D. McKeegan (University of California at Los Angeles)	OA_Mccain_00499_01
OAo4	14:00 - 14:15	Identifying characteristics of primordial and secondary products in SOM mass distributions extracted from CI, C2 ungrouped, CR and CM chondrites	*J.Isa (ELSI), F.-R. Orthous-Daunay (IPAG), V. Vuitton (IPAG), L. Bonal (IPAG), O. Poch (IPAG) and M. Zolensky (JSC)	OA_Isa_00619_01
OAo5	14:15 - 14:30	High-pressure minerals in CB carbonaceous chondrites	*Masaaki Miyahara (Hiroshima Univ.), Eiji Ohtani (Tohoku Univ.), Akira Yamaguchi (NIPR) and Naotaka Tomioka (JAMSTEC)	OA_Miyahara_00204_01
OAo6	14:30 - 14:45	Infrared spectroscopy of astromaterials with nanoscale resolution	*Mehmet Yesiltas (Kirklareli University), Timothy D. Glotch (Stony Brook University) and Bogdan Sava (Neaspec GmbH)	OA_Yesiltas_00557_01
OAo7	14:45 - 15:00	Formation of spherical iron oxide minerals by oxidative hydrothermal alteration from metallic spherules: Implications for hematite spherules and surface conditions of Mars	*Huimin Shao (Kumamoto University), Hiroshi Isobe (Kumamoto University), Ginga Kitahara (Kumamoto University) and Akira Yoshiasa (Kumamoto University)	OA_Shao_00518_01
	15:00 - 15:15	Break		
Chair: Naoya Imae (NIPR)				
OAo8	15:15 - 15:30	Comprehensive study of shock metamorphism and $^{40}Ar/^{39}Ar$ ages in ordinary chondrites	*Atsushi Takenouchi (The Kyoto University Museum, Kyoto University), Hirochika Sumino (Graduate School of Arts and Science, The University of Tokyo) and Akira Yamaguchi (National Instutute of Polar Research)	OA_Takenouchi_00593_01
OAo9	15:30 - 15:45	The effect of fluid mobilization on the budget and distribution of rare earth elements in Antarctic H chondrites	*Ryoga Maeda (Virije Universiteit Brussel), Steven Goderis (Virije Universiteit Brussel), Thibaut Van Acker (Ghent University), Frank Vanhaecke (Ghent University), Akira Yamaguchi (National Institute of Polar Research), Vinciane Debaille (Universite libre de Bruxelles) and Philippe Claeys (Vrije Universiteit	OA_Maeda_00288_01
OAo10	15:45 - 16:00	Thermal and shock history of diogenites based on the occurrence of silica minerals	*Rei Kanemaru (Institute of Space and Astronautical Science), Akira Yamaguchi (National Institute of Polar Research), Naoya Imae (National Institute of Polar Research) and Atsushi Takenouchi (Kyoto University)	OA_Kanemaru_00618_01

OAo11	16:00 - 16:15	Determination of the real size distribution of chondrules based on the measured size distributions in thin sections	*József Vanyo (Eszterhazy Karoly Catholic University, Faculty of Natural Sciences, Institute of Chemistry and Physics, Department of Physics), Arnold Gucsik (Eszterhazy Karoly Catholic University, Faculty of Natural Sciences, Institute of Chemistry and Physics, Department of Physics), Arpad Csamer (University of Debrecen, Cosmochemistry Research Group, Department of Mineralogy and Geology, Institute for Earth Sciences) and Jan Sztakovics (Eszterhazy Karoly Catholic University, Faculty of Natural Sciences, Institute of Chemistry and Physics, Department of	OA_Vanyo_00562_01

Poster presentations (1 November - 18 November)

OAp1	Multiscale characterization of Asuka 12169 meteorite - rehearsal of Hayabusa2 returned sample analysis -	*Masayuki Uesugi (JASRI/SPring-8), M. Ito (JAMSTEC Kochi), N. Tomioka (JAMSTEC Kochi), N. Imae (NIPR), A. Yamaguchi (NIPR), M. Kimura (NIPR), N. Shirai (Tokyo Met. Univ.), T. Ohigashi (UVSOR/IMS), M-C. Liu (UCLA), R.C. Greenwood (Open Univ.), K. Uesugi (JASRI/SPring-8), A. Nakato (JAXA-ISAS), K. Yogata (JAXA-ISAS), H. Yuzawa (UVSOR/IMS), Y. Kodama (MWJ), M. Yasutake (JASRI/SPring-8), K. Hirahara (Osaka Univ.), A. Takeuchi (JASRI/SPring-8), I. Sakurai (Nagoya Univ.), I. Okada (Nagoya Univ.), Y. Karouji (JAXA-ISAS), T. Yada (JAXA-ISAS) and M. Abe (JAXA-ISAS)	OA_Uesugi_00609_01
OAp2	Characterizing the Ryugu samples using the laboratory-based XRD and the meteorite collections at NIPR	*N. Imae (NIPR), A. Yamaguchi (NIPR), M. Kimura (NIPR), M. Ito (JAMSTEC Kochi), N. Tomioka (JAMSTEC Kochi), M. Uesugi (JASRI/SPring-8), N. Shirai (Tokyo Met. Univ.), T. Ohigashi (UVSOR/IMS), M-C. Liu (UCLA), R.C. Greenwood (Open Univ.), K. Uesugi (JASRI/SPring-8), A. Nakato (JAXA-ISAS), K. Yogata (JAXA-ISAS), H. Yuzawa (UVSOR/IMS), Y. Kodama (MWJ), M. Yasutake (JASRI/SPring-8), K. Hirahara (Osaka Univ.), A. Takeuchi (JASRI/SPring-8), I. Sakurai (Nagoya Univ.), I. Okada (Nagoya Univ.), Y. Karouji (JAXA-ISAS), T. Yada (JAXA-	OA_Imae_00205_02
OAp3	What is type 3.0 of chondrites?	*Makoto Kimura (National Institute of Polar Research)	OA_Kimura_00008_01
OAp4	Chemical analyses of Fe - rich chondrule phases in Kaba (CV3) carbonaceous - chondrite. Implications on the bulk elemental composition of terrestrial planetary cores	*P. Futo (University of Debrecen, Cosmochemistry Research Group, Department of Mineralogy and Geology) and A. Gucsik (Faculty of Natural Sciences, Institute of Chemistry and Physics, Department of	OA_Futo_00080_02
OAp5	On the bulk mineralogical composition of carbonaceous chondrites in low-Mg/Si planetary systems	*Peter Futo (University of Debrecen, Cosmochemistry Research Group, Department of Mineralogy and Geology) and Arnold Gucsik (Eszterházy Károly Catholic University, Faculty of Natural Sciences, Institute of Chemistry and Physics, Department of Physics)	OA_Futo_00080_01
OAp6	An attempt for estimating aqueous alteration environment from Raman spectra of iron sulfide	*Keisuke Narahara (Department of Chemistry, Graduate School of Science, Tokyo University of Science), Shu-hei Urashima (Department of Chemistry, Graduate School of Science, Tokyo University of Science), Akira Yamaguchi (National Institute of Polar Research), Naoya Imae (National Institute of Polar Research) and Hiroharu Yui (Department of Chemistry, Graduate School of Science, Tokyo University of	OA_Narahara_00547_01
OAp7	Identifying Polymorphs of Serpentine with Micro-Raman Spectroscopy	*Aruto Kashima (Tokyo University of Science), Shu-hei Urashima (Tokyo University of Science) and Hiroharu Yui (Tokyo University of Science)	OA_Kashima_00524_01
OAp8	Erg Chech 002 - A New Member of the (Trachy-) Andesite Meteorite Clan	*Viktor H Hoffmann (Faculty of Geosciences, Dep. Earth and Environmental Sciences, Univ. Munich / Germany), Phillipe Schmitt-Kopplin (Helmholtz-Center, Munich, Germany), Melanie Kaliwoda (Mineralogical State Collection Munich, SNSB, Germany) and Wolfgang Schmahl (Faculty of Geosciences, Dep. Earth and Environmental Sciences, Univ. Munich, Germany)	OA_Hoffmann_00587_01

OAp9	Chemical classifications of nine new iron meteorites from Yamato Mountains, Balchen and Nansen Ice field	*Naoki Shirai (Tokyo Metropolitan University), Akira Yamaguchi (National Institute of Polar Research), Makiko Haba (Tokyo Institute of Technology) and Shun Sekimoto (Institute for Integrated Radiation and Nuclear Science, Kyoto University)	OA_Shirai_00275_01

Lithium, and boron isotopic compositions of chondrule olivine from Yamato 81020, Asuka 12236 and QUE 97008 chondrites

Nozomi Matsuda[1]and Ming-Chang Liu[1]
[1]*Department of Earth, Planetary, and Space Sciences, University of California, Los Angeles, CA90095, USA*

Introduction:

How the Solar System derived its boron isotopic composition of $^{11}B/^{10}B = 4$ (inferred from the CI chondrites; Zhai et al., 1996) is still poorly understood. It is known that the majority of boron in the Galaxy is produced by spallation reactions between the Galactic Cosmic Rays (GCRs) and C-N-O nuclei in the interstellar medium (ISM), but the resulting $^{11}B/^{10}B$ ratio of 2.5 is significantly lower than the Solar System average (and elsewhere in the solar neighborhood), indicating that extra ^{11}B was added during or prior to Solar System formation (e.g., Reeves et al., 1970; Meneguzzi et al., 1971). Two nucleosynthetic processes capable of yielding components with high $^{11}B/^{10}B$ (>4) include low-energy (<10 MeV) irradiation (Bloemen et al., 1994) and the neutrino process during a supernova explosion (e.g., Yoshida et al., 2005); however, it is not clear which of the two sources was the dominant one. Lithium could help shed light on this question because this element is co-produced alongside boron by these processes with markedly different production ratios. Irradiation, regardless of the projectile energies, yields $^{7}Li/^{6}Li = 1.5$ (e.g., Meneguzzi., 1971), whereas the neutrino process makes almost pure ^{7}Li ($^{7}Li/^{6}Li$ >1,000) (e.g., Woosley et al., 1990). Therefore, a quantitative understanding of the relationship between $^{7}Li/^{6}Li$ and $^{11}B/^{10}B$ in the nebula can help better understand the distribution of the latter in the solar nebula from which the origin of ^{11}B-rich components could be constrained. Although there have been several studies about Li and B isotopes in chondrite components, only Chaussidon and Robert (1998) reported a correlated analysis result of the two systems in 3 chondrules from the ordinary chondrite Semarkona. In this study, we expand the correlated Li-B isotope measurements to chondrules from other pristine chondrites to better assess the distribution of $^{11}B/^{10}B$ in the nebula. Some preliminary results are reported here.

Sample and analytical methods:

Polished thin sections of Yamato (Y) 81020 (CO3.05), Asuka (A) 12236 (CM2.9), and QUE 97008 (L3.05) chondrites were examined to identify Type I porphyritic olivine-pyroxene (POP) chondrules through textures and chemical compositions by using a scanning electron microscope (SEM, Tescan Vega) equipped with an energy dispersive spectrometer (EDS) at UCLA. We focused on highly forsteritic olivine because it excludes beryllium, making its Li and B isotopes free of radiogenic ^{7}Li and ^{10}B from the decay of short-lived ^{7}Be and ^{10}Be, respectively. Even though the chondrules were selected from some of the most pristine chondrules, to ensure they have not been affected by parent body alteration, we first performed high precision 3-oxygen isotope measurements with the CAMECA ims-1290 ion microprobe, and then Li-B isotope analyses, all in multicollection mode.

Result and discussion:

All three chondrules studied here belong to Type I POP and appear to have internally homogeneous $\Delta^{17}O$, suggestive of the absence of aqueous alteration effects. The chondrule in Y-81020 contains forsteritic olivine characterized by $\Delta^{17}O$ value of ~ −5.1 ± 0.8‰ (2SD) and low-Ca pyroxene layers along the chondrule periphery. $\delta^{7}Li$ in olivine ranges from 6.4‰ to 15.5‰, while $\delta^{11}B$ shows a large spread ranging from −6.8‰ to 43.9‰. The A-12236 chondrule consists of olivine ($\Delta^{17}O$ values of ~ −4.8 ± 0.6‰ (2SD)) and low-Ca pyroxene phenocrysts. The $\delta^{7}Li$ and $\delta^{11}B$ values in olivine are in the range of −15.3‰ to 12.6‰ and −2.3‰ to 36.4‰, respectively. The QUE 97008 chondrule shows a similar texture to the chondrule in Y-81020, and its olivine has an average $\Delta^{17}O$ value of ~1.0 ± 0.9‰ (2SD). Olivine shows a $\delta^{7}Li$ variation from 3.9‰ to 25.1‰, and a larger $\delta^{11}B$ range of 4.9‰ to 50.8‰. We will discuss the meaning of $\delta^{7}Li$ and $\delta^{11}B$ variations in these chondrules in the meeting.

References:

Bloemen H., Wijnands R., Bennett K., Diehl R., Hermsen W., Lichti G., Morris D., Ryan J., Schonfelder V., Strong A. W., Swanenburg B. N., de Vries C. and Winkler C., COMPTEL observations of the Orion complex: evidence for cosmic-ray induced gamma-ray lines, Astron. Astrophys. 281, L5–L8, 1994.

Chaussidon M. and Robert F., $^{7}Li/^{6}Li$ and $^{11}B/^{10}B$ variations in chondrules from the Semarkona unequilibrated chondrite, Earth Planet. Sci. Lett. 164, 577–589, 1998.

Meneguzzi M., Audouze J. and Reeves H, The production of the elements Li, Be, B by galactic cosmic rays in space and its relation with stellar observations, Astron. Astrophys. 15, 337–359, 1971.

Reeves H., Fowler W. A. and Hoyle F., Galactic cosmic ray origin of Li, Be and B in stars, Nature 226, 727–729, 1970.

Woosley S. E., Hartmann D. H., Hoffman R. D. and Haxton W. C., The ν-process, Astrophys. J. 356, 272–301, 1990.
Yoshida T., Kajino T. and Hartmann D. H., Constraining the spectrum of supernova neutrinos from ν-process induced light element synthesis, Phys. Rev. Lett. 94, 231101, 2005.
Zhai M., Nakamura E., Shaw D. M. and Nakano T., Boron isotope ratios in meteorites and lunar rocks, Geochim. Cosmochim. Acta 60, 4877–4881, 1996.

Tarda: A highly aqueously altered meteorite from an outer Solar System asteroid?

Devin L. Schrader[1], Jemma Davidson[1], Dionysis Foustoukos[2], Conel M. O'D. Alexander[2], and Thomas J. Zega[3].

[1]*Center for Meteorite Studies, School of Earth and Space Exploration, Arizona State University, 781 East Terrace Road, Tempe, AZ 85287, USA.*

[2]*Earth and Planetary Laboratory, Carnegie Institution for Science, 5241 Broad Branch Road, Washington, DC 20015, USA.*

[3]*Lunar and Planetary Laboratory, University of Arizona, Tucson, Arizona 85721, USA.*

Introduction: Tarda is an ungrouped type 2 carbonaceous (C2-ung) chondrite that fell in Morocco on August 25th, 2020 near the village of Tarda (Gattacceca et al., 2021). King et al. (2021) found that Tarda is: (1) dominated by phyllosilicates, with minor amounts of olivine, magnetite, Fe-sulfides, and dolomite; (2) is distinct from CI and CY chondrites; and (3) displays no evidence for heating. Based on bulk isotopic compositional similarities with Tagish Lake, King et al. (2021) and Marrocchi et al. (2021) concluded that Tarda is similar to the C2-ung Tagish Lake and the Tagish Lake-like meteorites MET 00432 and WIS 91600 (Hiroi et al., 2008; Nakamura et al., 2013; Yamanobe et al., 2018; Ushikubo and Kimura, 2021). These Tagish Lake-like meteorites may be samples from D-type asteroid(s), which potentially formed in the outer Solar System between 8 and 13 AU (Hiroi et al., 2008; Yamanobe et al., 2018; Bryson et al., 2020; Marrocchi et al., 2021). These four similar carbonaceous chondrites are more numerous than the three samples required to define a grouplet, and only one meteorite shy of the five required to define a new meteorite group. To further constrain the compositions and petrology of this rare material, we determined the petrography, bulk H-C-N isotopic compositions, and *in situ* chemical compositions of metals, sulfides, and chondrule silicates.

Samples and Analytical Procedure: We analyzed two polished mounts of Tarda prepared from two separate stones (ASU 2149_C1 and 2149_C2) that were collected within days of the fall. X-ray element maps, high-resolution electron images, and chemical compositions were obtained with the JEOL-8530F Hyperprobe electron microprobe analyzer (EPMA) at Arizona State University (Figs. 1 and 2) and the Cameca SX-100 EPMA at the University of Arizona (UA), following procedures described in Schrader and Zega (2019). Chondrule sizes were measured in full polished section backscattered electron images and X-ray element maps using image measurement tools in Adobe Photoshop®. Bulk H, C, and N abundances and isotopic compositions were determined from a 1.03 gram homogenized interior sample (no fusion crust) at Carnegie Institution for Science following procedures of Alexander et al. (2007).

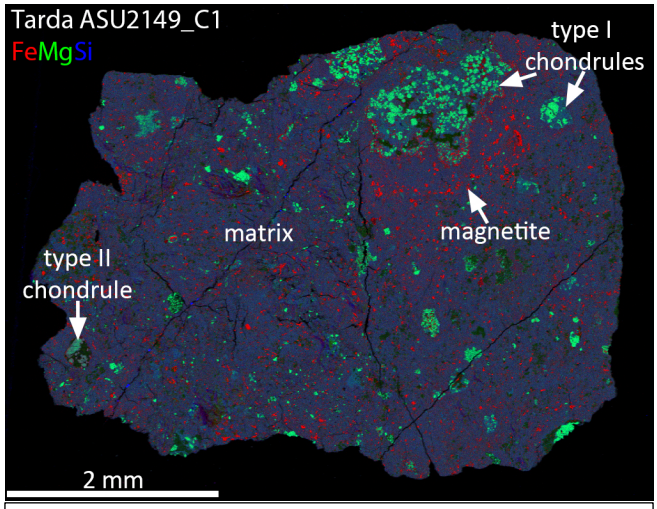

Figure 1. FeMgSi RGB X-ray element map of Tarda.

Results: Tarda has a bulk isotopic and elemental composition of $\delta^{13}C$ = 8.0‰ (4.17 wt.% C), $\delta^{15}N$ = 62‰ (0.297 wt.% N), and δD = 608‰ (0.916 wt.% H), yielding a bulk C/H (wt.%) ratio of 4.55. The *in situ* mineral compositions and petrography of the two polished mounts are indistinguishable from one another, therefore, mineral compositions and petrographic observations are presented together. We identified 18 FeO-poor (type I) and two FeO-rich (type II) chondrules, all of which are porphyritic and highly aqueously altered (no remaining unaltered glass and altered phenocrysts). One type II chondrule is nearly completely pseudomorphically replaced by phyllosilicates. Type II chondrules are significantly less abundant than type I chondrules (e.g., Fig. 1). Chondrule sizes of the twenty chondrules measured ranged from 0.11 to 1.30 mm (mean 0.27±0.12; mean±2SE). Many FeO-poor olivine fragments were observed in the matrix, which we conclude are fragments of type I chondrules, but their sizes were not measured. The composition of chondrule olivine is $Fa_{0.6–55.7}$, with Fe/Mn ratios ranging from 5–134 (# analyses = n = 65). The Fe-sulfides observed include both Fe-depleted pyrrhotite (mean Fe/S at.% ratio = 0.87, n= 14) and pentlandite (n = 18). Rare Fe,Ni metal in a type I chondrule was analyzed, with Ni = 5.6 – 6.2 wt.% and Co = 0.20 – 0.24 wt.% (n = 2).

Discussion: The bulk isotopic and elemental compositions of H, C, and N indicate that Tarda is very similar to analyses of Tagish Lake from Alexander et al. (2012), similar to the observation of Marrocchi et al. (2021). The mean at.% Fe/S ratio of Ni-poor (<1 wt.% Ni) pyrrhotite in Tarda is 0.87, which indicates a high degree of aqueous alteration consistent with that seen in CM1/2 and CI chondrites by Schrader et al. (2021). Pyrrhotite-pentlandite geothermometry via phase diagram analysis (e.g.,

Schrader et al., 2016) shows sulfide equilibration temperatures of approximately 100–135°C, which is also consistent with formation of the sulfides during low-temperature aqueous alteration, and provides an estimate for the minimum parent asteroid alteration temperature of Tarda. This is consistent with the observation of King et al. (2021) that Tarda has not been heated. Following the work of Kimura et al. (2008), the low Co content of Ni-poor Fe,Ni metal also indicates that the sample has not been noticeably heated. The mean chondrule size of 0.27±0.12 mm is most similar to that of CM chondrites (i.e., 0.27 mm; Rubin and Wasson, 1986). Fe-Mn systematics of chondrule olivine can help identify genetic relationships between groups (e.g., Berlin et al., 2011; Schrader et al., 2020). The Fe-Mn compositions of chondrule olivine in Tarda are most similar to that of CO and CM chondrites, possibly due to similarities in the formation conditions and/or formation region of their chondrules. While the distinct bulk O-isotope composition (Gattacceca et al., 2021) and H-C-N compositions (Marrocchi et al., 2021; this study) exclude the possibility that Tarda is a CM chondrite, Tarda's chondrules may have formed under similar conditions and from similar precursor materials, potentially in a similar formation region. In addition to being a fascinating new C2-ung chondrite similar to Tagish Lake, Tarda is a highly hydrated carbonaceous chondrite that will likely provide a comparison to the hydrated samples returned by Hayabusa2 and OSIRIS-REx.

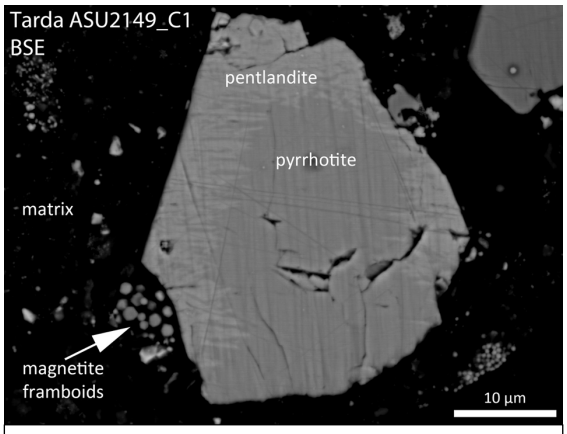

Figure 2. BSE of pyrrhotite-pentlandite intergrowth.

References

Alexander C.M.O'D. et al., The origin and evolution of chondrites recorded in the elemental and isotopic compositions of their macromolecular organic matter, Geochim. Cosmochim. Acta, 71, 4380–4403, 2007.

Alexander C.M.O'D. et al., The provenances of asteroids, and their contributions to the volatile inventories of the terrestrial planets, Science, 337, 721–723, 2012.

Berlin J. et al., Fe-Mn systematics of type IIA chondrules in unequilibrated CO, CR, and ordinary chondrites, Meteorit. Planet. Sci., 46, 513–533, 2021.

Bryson J. F. J. et al., Evidence for asteroid scattering and distal Solar System Solids from meteorite paleomagnetism, ApJ, 892, 126, 2020.

Gattacceca J. et al., The Meteoritical Bulletin, No. 109, Meteorit. Planet. Sci., 56, 1626–1630, 2021.

Hiroi T. et al., Meteorite WIS 91600: A new sample related to a D- or T-type asteroid, LPSC, XXXVI, #1564 (abstract), 2005.

Kimura K. et al., Fe-Ni metal in primitive chondrites: Indicators of classification and metamorphic conditions for ordinary and CO chondrites, Meteorit. Planet. Sci., 43, 1161–1177, 2008.

King, A. J. et al., The bulk mineralogy and water contents of the carbonaceous chondrite falls Kolang and Tarda, LPSC, 52, #1909 (abstract), 2021.

Marrocchi Y. et al., The Tarda meteorite: A window into the formation of D-type asteroids, ApJ Letters, 913, L9, 2021.

Nakamura T. et al., MET 00432: Another Tagish Lake-type carbonaceous chondrite from Antarctica, Meteorit. Planet. Sci., 48, #5122 (abstract), 2013.

Rubin A.E. and Wasson J. T., Chondrules in the Murray CM2 meteorite and compositional differences between CM-CO and ordinary chondrite chondrules, Geochim. Cosmochim. Acta 50, 307–315, 1986.

Schrader D. L. and Zega T. J., Petrographic and compositional indicators of formation and alteration conditions from LL chondrite sulfides, Geochim. Cosmochim. Acta, 264, 165–179, 2019.

Schrader D. L. et al., Widespread evidence for high-temperature formation of pentlandite in chondrites, Geochim. Cosmochim. Acta, 189, 359–376, 2016.

Schrader D. L. et al., Outward migration of chondrule fragments in the Early Solar System: O-isotopic evidence for rocky material crossing the Jupiter Gap? Geochim. Cosmochim. Acta, 282, 133–155, 2020.

Ushikubo T. and Kimura M., Oxygen-isotope systematics of chondrules and olivine fragments from Tagish Lake C2 chondrite: Implications of chondrule-forming regions in protoplanetary disk, Geochim. Cosmochim. Acta, 293, 328–343, 2019.

Yamanobe M. et al., Oxygen isotope reservoirs in the outer asteroid belt inferred from oxygen isotope systematics of chondrule olivines and isolated forsterite and olivine grains in Tagish Lake-type carbonaceous chondrites, WIS 91600 and MET 00432, Polar Sci., 15, 29–38, 2018.

Acknowledgements: We thank the ASU Center for Meteorite Studies for the samples used in this study, Laurence Garvie for sample preparation, and NASA grant NNX17AE53G (DLS PI, TJZ Co-I) for funding a portion of this research.

Carbonate minerals in the highly-altered A-12248 CM chondrite

Kaitlyn A. McCain[1], Ming-Chang Liu[1] and Kevin D. McKeegan[1]
[1]*University of California at Los Angeles*

The A-12248 meteorite was described in Meteorite Newsletter 26 as a highly-altered CM chondrite with a fracturing index of A/B, indicating the presence of exterior cracks on the surface (Yamaguchi et al. 2018). To date, no studies of this meteorite have been published. We received the thin section A-12248 51-3 on loan from NIPR and characterized it using secondary electron microscopy (SEM). We investigated its petrology using backscattered electron (BSE) and energy-dispersive X-ray spectroscopy (EDS) imaging. We directed particular attention to carbonate minerals, which precipitated from water during parent-body aqueous alteration and therefore recorded information about the fluid's composition and chemistry at the time of alteration.

A BSE image of the A-12248 51-3 section is shown in Figure 1. Chondrules in A-12248 are nearly completely pseudomorphed, though their outlines are still recognizable. In some cases, the original chondrule petrology can be discerned-a barred olivine chondrule can still be recognized despite complete replacement. No refractory inclusions could be identified. The matrix is dominated by small TCI (Tochilinite-Cronstedite Intergrowth) clumps. Rare, small Ca-phosphates are found in the matrix. Anhydrous silicates and FeNi metal are found only in the interior of the least altered chondrules. Magnetite is extremely rare, occurring only once. Though detailed EPMA data are not yet available, this section most closely resembles a CM 2.1 based upon the rarity of FeNi metal and the near-complete replacement of chondrule silicate (Rubin et al. 2007). However, we note that other classification criteria suggest a less-altered designation, as discussed below.

Small cracks in contact with the edge of the thin section are partially cemented with Ca and Mg carbonates, consistent with terrestrial alteration during Antarctic exposure (Jull et al. 1988, Tyra et al. 2007). Carbonate within or in contact with these veins will be excluded from future analyses and all other carbonates must be individually evaluated for a potential terrestrial component.

Ca-carbonate is the only indigenous carbonate type found in A-12248, in contrast with other CM 2.1 meteorites which often contain dolomite and other complex carbonates (Rubin et al. 2007). Based upon carbonate mineralogy, the classification CM 2.2 could be applied. Ca-carbonate is petrographically diverse, and is found inside pseudomorphed chondrules, replacing nearly entire chondrules, and isolated in the matrix. Most grains resemble Type II calcite in petrography, forming large (up to >100 μm) complex aggregates and containing small pores and sulfide inclusions (Tyra et al. 2011). Several inclusion-free grains isolated in the matrix resembling Type I calcite were found, but overall are much less abundant than those resembling Type II.

More detailed studies including light microscopy, cathodoluminescence imaging, elemental characterization by SEM-EDS, and 3 oxygen isotopic analyses using the Cameca ims-1290 at UCLA are planned for carbonates in A-12248. When possible, carbonates will be measured using an 800 pA Cs^+ beam with a precision of ± 0.5‰ (2SD) for both $\delta^{17}O$ and $\delta^{18}O$. Smaller carbonates and anhydrous silicates will be measured using a 40 pA Cs^+ beam with a precision of $\delta^{17}O$ ± 1.0 ‰ and $\delta^{18}O$ ± 1.6 ‰ (2SD). The Mn content of each Ca-carbonate will be measured using SEM-EDS and used to assess whether Mn-Cr dating can be performed.

Further results and details will be presented at the meeting.

References

Yamaguchi, A., Kimura, M., Imae, N., L. Pittarello, V. Debaille, S. Goderis, P. Claeys, Meteorite newsletter: Japanese/Belgian collection of Antarctic meteorites, Meteorite Newsletter, 26, 1-28, 2018.

A.J.T. Jull, S. Cheng, J.L. Gooding, M.A. Velbel, Rapid growth of magnesium-carbonate weathering products in a stony meteorite from Antarctica, Science, 242, 417-419, 1988.

M. A. Tyra, J. Farquhar, B. A. Wing, G. K. Benedix, A. J. T. Jull, T. Jackson, M. H. Thiemens, Terrestrial alteration of carbonate in a suite of Antarctic CM chondrites: Evidence from oxygen and carbon isotopes. Geochimica et Cosmochimica Acta, 71(3), 782-795, 2007.

A. Rubin, J. M. Trigo-Rodriguez, H. Huber, J. T. Wasson, Progressive aqueous alteration of CM carbonaceous chondrites, Geochimica et Cosmochimica Acta, 71(9), 2361-2382, 2007.

M. A. Tyra, J. Farquhar, Y. Guan, and L. A. Leshin. An oxygen isotope dichotomy in CM2 chondritic carbonates—A SIMS approach, Geochimica et Cosmochimica Acta, 77, 383-395, 2012

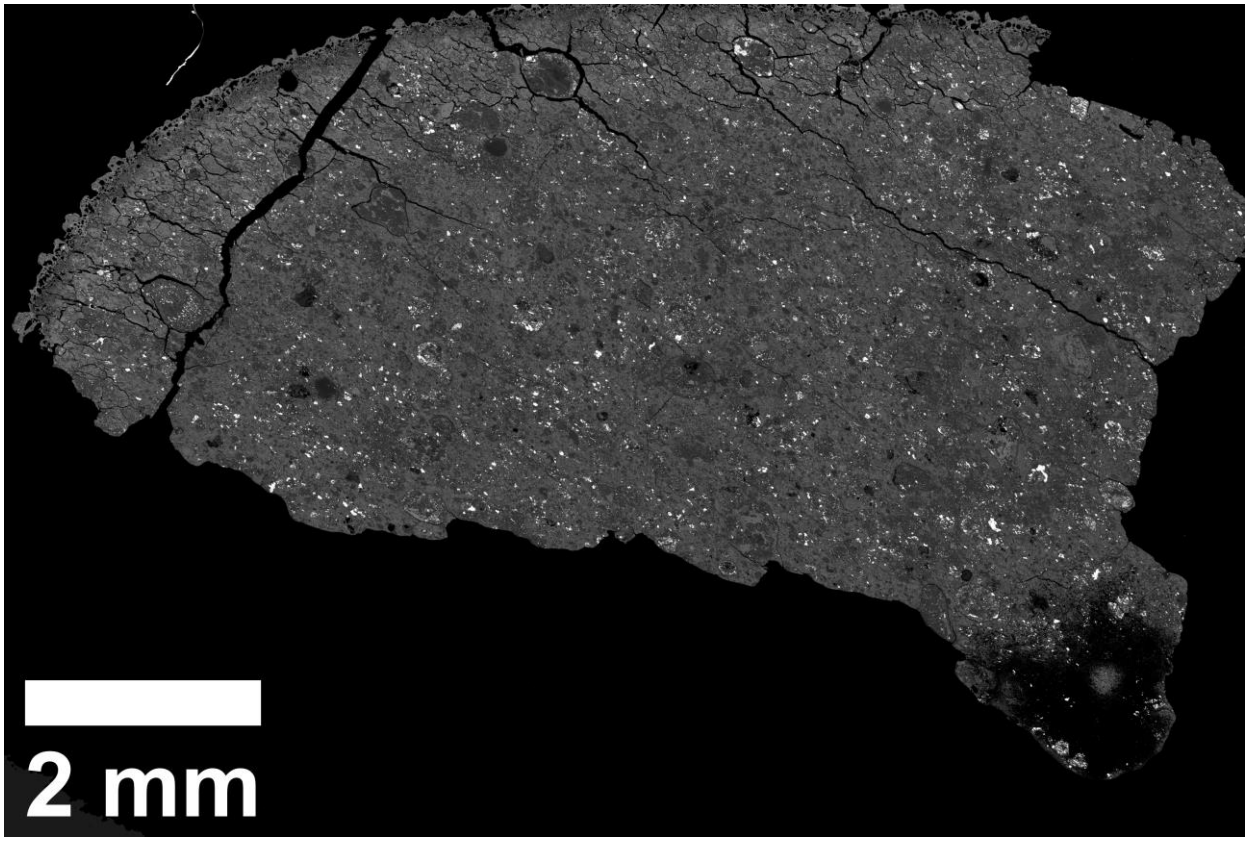

Figure 1. Back-scattered electron (BSE) image of A-12248 51-3. The fusion crusted surface is visible at the top and left of the section.

Identifying characteristics of primordial and secondary products in SOM mass distributions extracted from CI, C2 ungrouped, CR and CM chondrites.

J.Isa1, F.-R. Orthous-Daunay[2], V. Vuitton[2], L. Flandinet[2], L. Bonal[2], O. Poch[2], and M. Zolensky[3]

[1] *Earth-Life Science Institute, Tokyo Institute of Technology, Tokyo, Japan*

[2]*Univ. Grenoble Alpes, CNRS, IPAG, 38000 Grenoble, France CS 40700 38058 Grenoble Cedex 9, France*

[3]*NASA Johnson Space Center, Houston, TX 77058, USA*

The differences in chemistry, mineralogy, and structure of chondrites demonstrate the variations in time/space of their formation regions in the solar nebula and the subsequent evolution of their parent body. Naturally, one may expect to find some variations in the chondritic organics reflecting their different reservoirs in the solar nebula and the secondary modifications on asteroids [1]. Chondrite soluble organic matter (SOM) is complex, and the aqueous reactions on asteroids are thought to be where it was synthesized [2]. Our previous study of Tagish Lake (C2 ungrouped) showed that the primordial SOM could be distinguished from the parent body's secondary alteration through mass distribution. Also, we concluded that the complex nature of the primordial SOM was established before severe alteration on the asteroid and later became simplified on the asteroid [3]. However, it remains unclear if this conclusion can be generalized and applied to other chondrite groups. This study will show the variations and common SOM features among different chondrite groups and petrologic types by using the model from our previous study.

Sample and Method: Tarda (C2 ungrouped), Orgueil (CI), Murchison (CM2), EET 96029 (CM2), GRO 95577 (CR1), EET 92159 (CR2), GRA 06100 (CR2), GRO 03116 (CR2), and MIL 090657 (CR2) meteorite SOM, as well as chondrite organic simulant SOM, were used. We analyzed the methanol/toluene extract with the high-resolution Orbitrap mass spectrometer located at the Institut de Planétologie et d'Astrophysique de Grenoble (IPAG). We directly injected and ionized the SOM and its solvent by using an Electrospray Ionization (ESI) source. After spectra acquisition, post-processing data analysis tools with the name Attributor [4], which were developed in-house, were employed.

Preliminary Results: Tarda and the other type 2 chondrites' SOM mass distribution were well fit by using the model interpreted as the primordial SOM distribution in Tagish Lake. This match among the distribution patterns from different chondrite types implies the presence of a common organic reservoir or a common mechanism for SOM formation. The model fits better to Tarda SOM distribution than Tagish Lake ones; that implies that Tarda was less altered in the parent body than Tagish Lake, consistent with their minerlogies. Orgueil and GRO 95577 (CR1) share the common shape in their mass distribution of a few alkyl homologous series, and these unique features are apparent only in type 1 chondrites' extracts (Figure 1). In contrast to the mass distribution, SOM's elemental abundance was distinct among the different chondrite groups. In the presentation, we will discuss in detail the common features among the chondrite groups through the alteration on individual parent bodies based on the mass distribution and chemical formulae of detected ions.

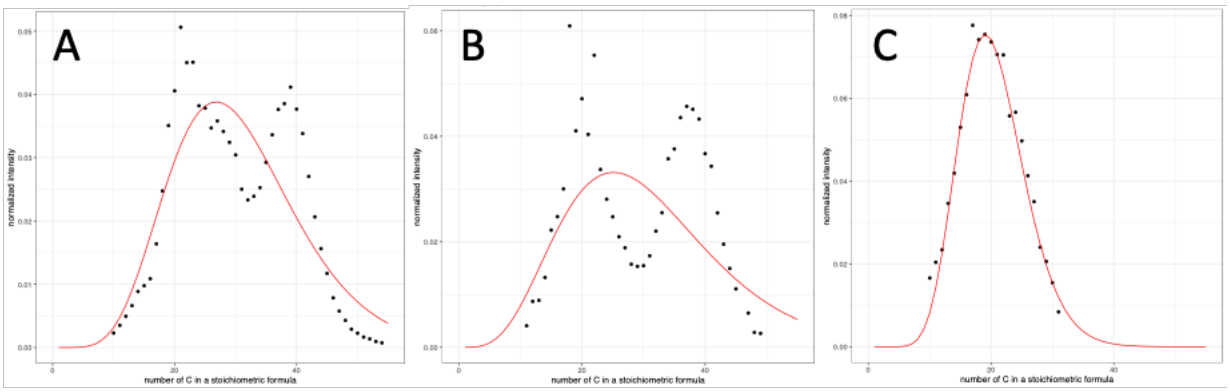

Figure 1: Selected CH_2 family intensity pattern from **A**: Orgueil, **B** GRO 95577 (CR1) and **C** Tarda (C2) extracts. Multimodal peaks appeared in the type-1. The red line is the best fit to the SZ model interpreted as the primordial SOM distribution in Tagish Lake.

References: [1] Naraoka and Hashiguchi (2019) Geochemical Journal, 53, 33-40, [2] Cronin and Chang, (1993) The Chemistry of Life's Origins pp 209-258 [3] Isa *et al.* (2021) The Astrophysical Journal Letters (accepted), [4] Orthous-Daunay, F. R. *et al.* (2019) Geochemical Journal, 53(1), 21-32.

High-pressure minerals in CB carbonaceous chondrites

Masaaki Miyahara[1], Eiji Ohtani[2], Akira Yamaguchi[3], Naotaka Tomioka[4]
[1]*Hiroshima University*, [2]*Tohoku University*, [3]*NIPR*, [4]*JAMSTEC*

It is widely accepted that carbonaceous chondrites are less shocked compared to ordinary chondrites. A high-pressure mineral, which is one of stark evidence for shock metamorphism, is ubiquitously found in ordinary chondrites (Miyahara et al. 2020, 2021 and references therein). By contrast, based on previous studies, only a few carbonaceous chondrites include a high-pressure mineral (Tomioka and Miyahara 2017 and references therein). Among carbonaceous chondrites, CB carbonaceous chondrite is a unique group because it consists mainly of metal and chondrule. Although the origin of CB carbonaceous chondrite has been under debate, some previous studies propose that CB carbonaceous chondrite may be formed through a planetesimal collision between carbonaceous chondrite and iron meteorite parent-bodies (Weisberg and Kimura, 2010). Most CB carbonaceous chondrites show evidence for melting, probably induced by shock metamorphism. In this study, we investigate a high-pressure mineral in four CB carbonaceous chondrites: Gujba, Bencubbin, NWA 1814, and NWA 4025 to clarify its history of shock metamorphism and origin using FEG-SEM, EMPA, and laser Raman spectroscope.

Gujba, Bencubbin, NWA 1814, and NWA 4025 consist of a chondrule, metal spherule, and matrix. The chondrule and metal spherule are deformed, and their sizes are 1–5 mm across. The chondrules have irregular fractures and consist mainly of olivine, low-Ca pyroxene, high-Ca pyroxene, and glass. The metal spherule consists of kamacite-taenite. Some metal spherules include a small amount of iron-sulfide patch. The kamacite-taenite and iron-sulfide have a eutectic texture in the patch. Other metal spherules include fragmented chondrules. The matrix consists of fragmented chondrules, and their outlines are rounded. The interstices of the fragmented chondrules are filled with fine-grained olivine and pyroxene, glass (or poorly crystallized material), and metallic iron.

The high-pressure polymorphs of olivine, pyroxene, and plagioclase are found mainly in the matrix of Gujba, Bencubbin, NWA 1814, and NWA 4025. Gujba includes wadsleyite, ringwoodite, akimotoite, majorite, Ca-bearing majorite, lingunite, and Na-pyroxene as a high-pressure mineral. Pyroxene-glass also occurs in the matrix, which may be vitrified bridgmanite. Also, Weisberg and Kimura (2010) and Garvie et al. (2014) found majorite-pyrope solid-solution, coesite, and diamond in Gujba. Considering the assemblage of high-pressure minerals, the shock pressure recorded in Gujba would be at 22–23 GPa. Bencubbin includes majorite, Ca-bearing majorite, and pyroxene-glass. The estimated shock pressure in Bencubbin is 15–22 GPa. NWA 1814 includes Na-pyroxene, coesite, and pyroxene-glass. The estimated shock pressure is 22–23 GPa. NWA 4025 includes majorite and pyroxene-glass and the estimated shock pressure is 22–23 GPa.

Our systematic investigations of Gujba, Bencubbin, NWA 1814, and NWA 4025 indicate that high-pressure minerals occur ubiquitously in the matrices of CB carbonaceous chondrites. The chondrules are deformed and fractured. The metal spherules are also deformed and include the fragmented chondrules. The matrices of CB carbonaceous chondrites consist of quenched melts and fragmented chondrules. CB carbonaceous chondrites likely experienced heavy shock metamorphism after metal spherules and chondrules were accumulated on the parent body. The estimated shock pressures based on high-pressure minerals are similar to each other. CB carbonaceous chondrites may be disrupted from the parent body simultaneously.

References

Garvie L.A.J., Németh P., & Buseck P.R. (2014). Transformation of graphite to diamond via a topotactic mechanism. Am Min 99:531–538.

Miyahara M., Yamaguchi A., Saitoh M., Fukimoto K., Sakai T., Ohfuji H., Tomioka N., Kodama Y., & Ohtani E. (2020). Systematic investigations of high-pressure polymorphs in shocked ordinary chondrites. Meteorit Planet Sci 55:2619–2651.

Miyahara M., Tomioka N., & Bindi L. (2021) Natural and experimental high-pressure, shock-produced terrestrial and extraterrestrial materials. Progress in Earth and Planetary Science, in press.

Tomioka N. & Miyahara M. (2017). High-pressure minerals in shocked meteorites. Meteorit Planet Sci 52:2017–2039.

Weisberg M.K. & Kimura M. (2010). Petrology and Raman spectroscopy of high pressure phases in the Gujba CB chondrite and the shock history of the CB parent body. Meteorit Planet Sci 45:873–884.

Infrared spectroscopy of astromaterials with nanoscale resolution

Mehmet Yesiltas[1], Timothy D. Glotch[2], Bogdan Sava[3]
[1]*Faculty of Aeronautics and Space Sciences, Kirklareli University, Kirklareli, Turkey*
[2]*Department of Geosciences, Stony Brook University, Stony Brook, New York, USA*
[3]*Neaspec GmbH, D-85540 Haar, Munich, Germany*

Introduction: Astromaterials are invaluable samples for understanding the formation of our solar system. Investigation of returned asteroid particles, micrometeorites, and meteorites significantly contributes to our understanding of the early solar system. Carbonaceous chondrites, for instance, are some of the most primitive extraterrestrial samples, and they retain records of their origin, formation, evolution and post-accretionary processes. Their heterogeneous chemical composition includes a wide range of organic compounds as well as minerals. Organic molecules are typically sub-micron in size [1,2]. Organic nanoglobules are even smaller (50–500 nm). [3,4]. As such, novel analytical techniques with nanoscale spatial resolution are required to detect and characterize such organic matter within meteorites. It is also important to preserve the petrographic context and not alter the organic matter during the investigation. Conventional Fourier transform infrared (FTIR) spectroscopy is a non-destructive analytical technique; however, its spatial resolution is not high enough to detect and identify spectral signatures of organic molecules that are smaller than a micrometer. In contrast, nanoscale near-field infrared (nano-FTIR) spectroscopy can non-destructively characterize organic matter and mineral phases in extraterrestrial samples with nanoscale spatial resolution (e.g., 5-7). It is not affected by the optical diffraction limit, independent of the wavelength, preserves the context since it does not require powdered or chemically processed samples. Therefore, nano-FTIR spectroscopy is a powerful analytical tool for the investigation of constituents of extraterrestrial materials. In this work, we report nano-FTIR spectral results of organic matter identified in carbonaceous chondrites.

Technique: This work considers several carbonaceous chondrites that were prepared in the form of polished sections. We conducted our nano-FTIR spectroscopic experiments using a commercial s-SNOM nano-FTIR imaging and spectroscopy system (neaspec GmbH) equipped with mid-infrared broadband lasers. Spectra were collected within the 2000–650 cm^{-1} spectral range with ~20 nm spatial resolution. AFM scans were collected using a Pt coated neaspec cantilever tip that maps the surface topography. Sample drift was monitored constantly by checking the reference points on each sample.

Results:

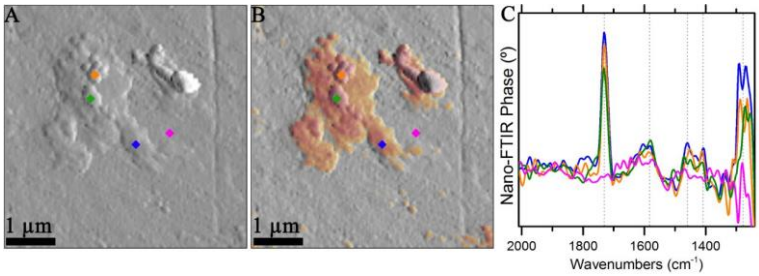

Figure 1. Identification of carbonyls. A and B respectively present mechanical and amplitude images of a region in DOM 08006 (CM3.0). Nano-FTIR spectra of the points indicated by diamonds in A and B are shown in C. The infrared band at 1730 cm^{-1} is due to carbonyls, which is absent in the pink spectrum that was collected within the matrix.

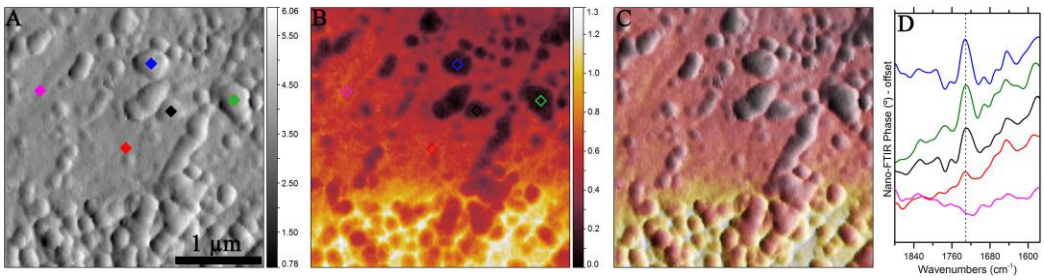

Figure 2. Identification of roughly spherical carbonyl nanoglobules in DOM 08006.

References

[1] Busemann et al. 2006; Science, 312,727-730. [2] Remusat et al. 2010, The Astrophysical Journal 713,1048. [3] Nakamura-Messenger, K. et al. 2006, Science, 314,1439-1442. [4] De Gregorio, B. T. et al. 2013, Meteoritics & Planetary Science, 48,904-928. [5] Kebukawa et al. 2019; PNAS, 116, 753-758. [6] Yesiltas et al. 2020, Meteoritics & Planetary Science, 55, 2404-2421. [7] Yesiltas et al. 2021, Scientific Reports, 11, 11656.

Formation of spherical iron oxide minerals by oxidative hydrothermal alteration from metallic spherules: Implications for hematite spherules and surface conditions of Mars

Huimin Shao[1], Hiroshi Isobe[1*], Ginga Kitahara[1], and Akira Yoshiasa[1]

[1] *Department of Earth and Environmental Sciences, Faculty of Advanced Science and Technology, Kumamoto University, Kumamoto, 860-8555, Japan.*

The formation mechanism of hematite spherules on Mars was widely discussed by researchers (e.g. Bowen et al., 2008; Fan et al., 2010). The discussion about the formation history of the hematite spherules could provide the Martian surface condition. In this study, oxidative hydrothermal alteration experiments on reproduced I-type (iron type) cosmic spherules were carried out to investigate the formation history of hematite spherules on Mars.

The starting material used in this study was reproduced I-type cosmic spherules formed by high-temperature heating and quenching experiments from Canyon Diablo iron meteorite (Shao et al., 2020) in a reduced atmosphere controlled by Ar (98%) and H_2 (2%) gas flow to protect from oxidation. The starting material shows a homogeneous composition with approximately 7 wt% Ni and 93 wt% Fe in the metallic phase. Detailed conditions of hydrothermal alteration experiments are shown in Table 1.

Table 1. Experimental conditions

Exp.	T (°C)	Dur (days)	pH	CO_2
1	100	10	7	×
2	100	10	4	×
3	100	30	7	×
4	100	30	4	×
5	150	10	7	√
6	150	10	4	×
7	150	30	7	√
8	150	30	7	×
9	150	100	7	×
10	150	100	4	×
11	200	10	7	×
12	200	10	4	×
13	200	30	7	√
14	200	30	7	×
15	200	100	7	×
16	200	100	4	×

Based on the observation of all the run products, we suggest that the Martian hematite spherules could be formed from metallic spherules produced in the ablation of iron meteorites during Martian atmospheric entry. The area with high-density Martian hematite spherules may be derived from an explosion and ablation events of large iron meteorites at a low altitude. The reproduced hematite on artificial I-type cosmic spherules formed in this study contains Ni content from 0.52 to 4.77 wt%. Thus, we suggest that the hematite spherules which were oxidized from metallic spherules originated from iron meteorites or I-type cosmic spherules typically have Ni content with a few wt.%. However, hematite spherules precipitated in the aqueous process only contain Ni less than tens of ppm (Bowen et al., 2008). If an obvious nickel content could be detected in Martian hematite spherules from future Martian missions, the Martian hematite spherules may be formed by oxidation of metallic spherules rather than precipitation from a fluid. Furthermore, it could be also suggested that the Martian hematite spherules deposit is not a suitable place to find the ancient river, not as researchers thought previously. In this study, we propose that the precursor of Martian hematite spherules should be metallic spherules derived from iron meteorites.

References

Bowen, B.B., Benison, K.C., Oboh-Ikuenobe, F.E., Story, S., Mormile, M.R., 2008. Active hematite concretion formation in modern acid saline lake sediments, Lake Brown, Western Australia. Earth and Planetary Science Letters 268, 52-63.

Fan, C., Xie, H., Schulze-Makuch, D., Ackley, S., 2010. A formation mechanism for hematite-rich spherules on Mars. Planetary and Space Science 58, 401-410.

Shao, H., Isobe, H., Miao, B., 2020. Reproduction of I-type cosmic spherules and characterization in an Fe-Ni-O system. Meteorit. Planet. Sci.

Comprehensive study of shock metamorphism and $^{40}Ar/^{39}Ar$ ages in ordinary chondrites

Atsushi Takenouchi[1], Hirochika Sumino[2] and Akira Yamaguchi[2]
[1] *The Kyoto University Museum, Kyoto University*
[2]*Graduate School of Arts and Science, The University of Tokyo*
[3]*National Institute of Polar Research (NIPR)*

Introduction

Ordinary chondrites have experienced shock metamorphism in various degrees. For example, L chondrites commonly contain high-pressure phases, indicating that those meteorites have metamorphosed under high-pressure and high-temperature (e.g., Tomioka and Miyahara 2017). Stöffler et al. (1991, 2018) classified such shock metamorphic degrees based on shock textures from unshocked (1) to highly shocked (6), and this classification is widely used to represent shock degrees efficiently. On the other hand, $^{40}Ar/^{39}Ar$ ages (hereafter Ar/Ar ages) have been measured to investigate impact histories in each meteorite group (e.g., Bogard 2011; Swindle et al. 2014). While several studies have discussed the degrees of impact events and their timing (e.g., Friedrich et al. 2014; Rubin 2004), the number of such research is still limited. Moreover, in general, observation of shock textures and their chronology were performed separately using different specimens. A comprehensive study investigating shock metamorphism and impact ages of many meteorites is needed to reveal impact histories during the solar system formation. Therefore, we have been analyzing both shock metamorphism and Ar/Ar ages of ordinary chondrites using identical specimens. Here, we report our results so far and discuss the impact histories of ordinary chondrites.

Samples and Methods

We prepared twenty-six H chondrites, three L chondrites, and three LL chondrites (Table 1). Part of them was bought from meteorites dealers, and the others were provided by the University of Tokyo and NIPR. We observed polished thin sections of each meteorite by an optical microscope and FE-SEM (JEOL JMS-7100F at NIPR). Chips of each meteorite were irradiated by neutrons at Institute for Integrated Radiation and Nuclear Science, Kyoto University. Ar/Ar analyses were performed using modified VG-3600 at the University of Tokyo. Detailed data reduction is described in Takenouchi et al. (2020).

Results

We summarize our observation results so far and obtained Ar/Ar ages in Table 1. Some Ar/Ar ages were previously reported in Takenouchi et al. (2020), and data from Swindle et al. (2014) are also shown. In this study, seven Ar/Ar ages are newly reported. Ar/Ar age spectrum of Mills is shown in Fig. 1 as an example. Shock stages were determined based on the classification suggested by Stöffler et al. (2018). Fig. 2 represents shock stages versus Ar/Ar ages as per Table 1. Meteorites with younger Ar/Ar ages (<4000 Ma) show higher shock stages (≥3), while shock stages of meteorites with older ages (>4000 Ma) are variable. Only two out of twenty-six H chondrites contain high-pressure phases indicating that high-pressure phases are less common in H chondrites than in L chondrites.

Discussion and Conclusion

In general, moderate to strong shock metamorphism is needed to completely reset Ar/Ar ages (e.g., Bogard et al. 1995), and unshocked meteorites should retain their formation ages. Therefore, the trend in Fig. 2 appears natural because strongly shocked meteorites have reset Ar/Ar ages and unshocked meteorites exhibit older ages. However, only weakly shocked meteorites such as Ochansk and Mills show relatively young ages around 4200 Ma (Fig. 2). Such Ar/Ar age is too young to represent the chondrites' formation age and should represent an impact age. Furthermore, those meteorites commonly show healed cracks, which formed during heating after the crack formation. Therefore, these meteorites may have experienced post-shock annealing to erase significant shock metamorphic textures similar to meteorites reported previously (Rubin 2004). Rubin et al. (2001) suggested that Portales Valley, whose Ar/Ar age is 4480±40 Ma, may also be annealed by shock event based on its textures. Therefore, these results indicate that impact events until ~4200 Ma were sometimes accompanied by strong post-shock annealing. On the other hand, meteorites with low shock stage and young Ar/Ar ages are not found so far, which possibly indicates that recent impact events (after at least 4200 Ma) rarely induced post-shock temperature strong enough to erase shock metamorphic textures. Such a difference in post shock annealing can be attributable to changes in impact conditions at around 4200 Ma. To ensure the trend of shock metamorphism and reveal impact histories of meteorites, further analyses with increasing samples is required.

References

Bogard D. D., Garrison D. H., Norman M., Scott E. R. D., and Keil K. 1995. 39Ar40Ar age and petrology of Chico: Large-scale impact melting on the L chondrite parent body. *Geochimica et Cosmochimica Acta* 59:1383–1399.

Bogard D. D. 2011. K-Ar ages of meteorites: Clues to parent-body thermal histories. *Chemie der Erde* 71:207–226. http://dx.doi.org/10.1016/j.chemer.2011.03.001.
Friedrich J. M., Rubin A. E., Beard S. P., Swindle T. D., Isachsen C. E., Rivers M. L., and Macke R. J. 2014. Ancient porosity preserved in ordinary chondrites: Examining shock and compaction on young asteroids. *Meteoritics and Planetary Science* 49:1214–1231.
Rubin A. E., Ulff-Moller F., Wasson J. T., and Carlson W. D. 2001. The Portales Valley meteorite breccia: Evidence for impact-induced melting metamorphism of an ordinary chondrite. *Geochimica et Cosmochimica Acta* 65:323–342.
Rubin A. E. 2004. Postshock annealing and postannealing shock in equilibrated ordinary chondrites : Implications for the thermal and shock histories of chondritic asteroids. 68:673–689.
Stöffler D., Keil K., and Edward R.D S. 1991. Shock metamorphism of ordinary chondrites. *Geochimica et Cosmochimica Acta* 55:3845–3867.
Stöffler D., Hamann C., and Metzler K. 2018. Shock metamorphism of planetary silicate rocks and sediments: Proposal for an updated classification system. *Meteoritics and Planetary Science* 53:5–49.
Swindle T. D., Kring D. A., and Weirich J. R. 2014. 40Ar/39Ar ages of impacts involving ordinary chondrite meteorites. In *Advances in 40Ar/39Ar Dating: from Archaeology to Planetary Sciences*. pp. 333–347.
Takenouchi A., Sumino H., and Yamaguchi A. 2020. Shock metamorphism and Ar-Ar ages of ordinary chondrites. *11th Polar Science symposium* OPp1.
Tomioka N., and Miyahara M. 2017. High-pressure minerals in shocked meteorites. *Meteoritics and Planetary Science* 52:2017–2039.

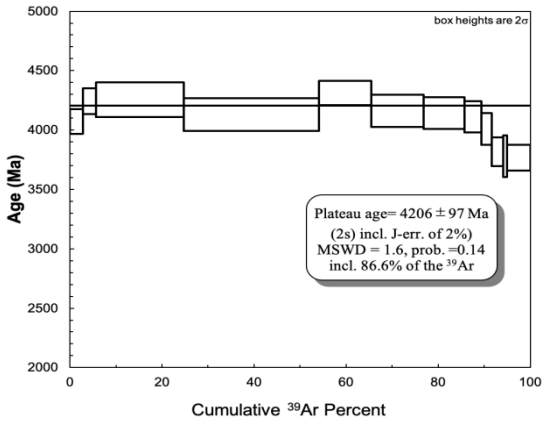

Fig. 1 Ar/Ar age spectrum of Mills showing a plateau age of 4206±97 Ma.

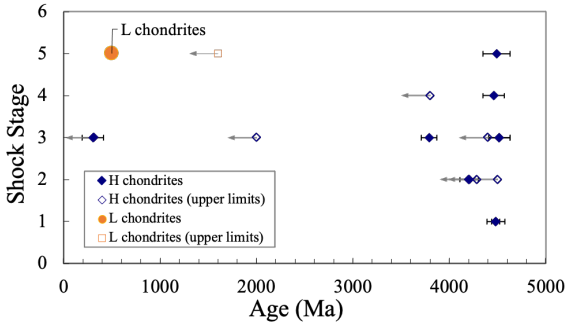

Fig. 2 Shock stages and Ar/Ar ages of meteorites studied (Blue: H chondrites, Orange: L chondrites). Error bars (2 σ) are shown, and only younger ages in Table 1 are plotted with arrows as Ar/Ar ages in this graph. The impact event of L chondrites at 0.5 Ga (e.g., Swindle et al. 2014) is also shown.

Table 1 Thermal metamorphic types, shock stages and Ar/Ar ages of meteorites used in this study. Errors in Ar/Ar ages are 2σ.

Name	TYPE	Shock Stage	Age (Ma)	Name	TYPE	Shock Stage	Age (Ma)
Tulia(a)	H3-4	3	<2000-4000	Chergach	H5	4	
Y-75028	H3-6	3		Mills	H6	2	4206±97
Y-791428	H3.7	1		Ozona	H6	2	<4500**
Y-790460	H3.7	3	4520±110	Portales Valley	H6	1	4480±40*
Ochansk	H4	2	<4200**	A 10174	H6	3	
Salaices	H4	3	<4400**	A 12363	H6	2	
Wellman-c	H4	4	<3800**	Y 981909	H6	5+	
Hassayampa	H4	3	4520±110	Y-791775	H6-melt rock	2	<4300
Kesen	H4	3		Y-75100	H6	5+	<4490±140*
Jilin	H5	3	<300-400 <3800	Tassédet 004	H5-melt rock	4	
Nuevo Mercurio	H5	1	4481±92**	Seagraves (c)	L6	5+	<1600-2900**
Gao-Guenie	H5	3	303±110*	Y 000775	L6	5+	
Nadiabondi	H5	3		Y-790521	L-melt rock	3	
Plainview (1917)	H5	4	4460±110	Y-790144	LL7	3	
Forest City	H5	3		Y-790519	LL-melt rock	2	
Y-794046	H5?	3	3790±80*	Y-790964	LL-melt rock	3	

*Swindle et al. (2014) and references therein **Takenouchi et al. (2020) after further data reduction +contains high-pressure phases

The effect of fluid mobilization on the budget and distribution of rare earth elements in Antarctic H chondrites

Ryoga Maeda[1, 2], Steven Goderis[1], Thibaut Van Acker[3], Frank Vanhaecke[3],
Akira Yamaguchi[4], Vinciane Debaille[2] and Phillippe Claeys[1]
[1]*Analytical-, Environmental-, and Geo-Chemistry, Vrije Universiteit Brussel, Belgium*
[2]*Laboratoire G-Time, Université libre de Bruxelles, Belgium*
[3]*Atomic & Mass Spectrometry Research Unit, Department of Chemistry, Ghent University, Belgium*
[4]*National Institute of Polar Research, Japan*

Introduction

Rare earth elements (REEs) are universally used for understanding planetary processes such as silicate differentiation and are often considered to be relatively immobile. Despite this overall immobility, previous studies on the weathering effects on REEs have demonstrated that terrestrial weathering including Antarctic alteration can modify original REE compositions both in terms of absolute concentrations and isotopic ratios [*e.g.*, 1]. In addition, Maeda *et al*. [2] put forward that Antarctic alteration may be significantly more complex than previously acknowledged. The detailed mechanisms of the alteration, however, remain poorly understood. In this study, H chondrites (HCs) with various degrees of weathering are investigated to reveal the underlying mechanisms through the use of several types of *in-situ* measurements.

Experimental

Polished thick sections (PTSs) were prepared for ten Antarctic HCs, two HCs collected from hot deserts, and four fall HCs provided by the Royal Belgian Institute of Natural Sciences (RBINS), Belgium, and the National Institue of Polar Research (NIPR), Japan. Firstly, these PTSs were analyzed using micro-X-ray fluorescence spectrometry (μXRF) at the Vrije Universiteit Brussel (VUB), Belgium, to obtain maps showing the distributions of major elements. Secondly, back-scattered electrons (BSE) images of each sample were acquired using a field emission-scanning electron microscope (FE-SEM) equipped with an energy-dispersive spectrometer (EDS) at NIPR. Once the constituent minerals in the samples were identified based on the elemental maps and BSE images obtained, an electron probe micro analyzer (EPMA) at NIPR was used for the determination of major elemental abundances in each constituent mineral. After the EPMA analysis, trace element mapping was conducted for selected samples using laser ablation-inductively coupled plasma-time of flight-mass spectrometry (LA-ICP-TOF-MS) at Ghent University, Belgium. Finally, the abundances of REEs and other trace elements of choice were determined for constituent minerals and cracks using single point drilling for the minerals and line scans for the cracks by LA-ICP-MS at NIPR.

Results and Discussion

According to the result of the trace element mapping using LA-ICP-TOF-MS, a considerable amount of REEs resides in the cracks within Asuka (A) 09618 (H5), which is severely weathered and categorized to C following the weathering index (WI), as shown in Fig. 1. Other highly weathered samples, *e.g.*, A 09516 (H6; WI: C) and Sahara 97035 (H5; WI: W2), also show such a deposition of Ce in cracks, but this is not observed for the other REEs. Based on the REE abundances in cracks as determined using LA-ICP-MS line scanning, some cracks display elevated REE abundances relative to the bulk rock (Fig. 2 as an example). These REE-enriched cracks usually also contain high Th and U abundances. Considering the P_2O_5/SiO_2 in cracks (Fig. 2), most of the high REE-cracks must be explained by a nugget effect of Ca-phosphates, as crack-1 and crack-2 show high REE, Th, and U abundances with a high P_2O_5/SiO_2, while crack-4 displays low abundances in these elements

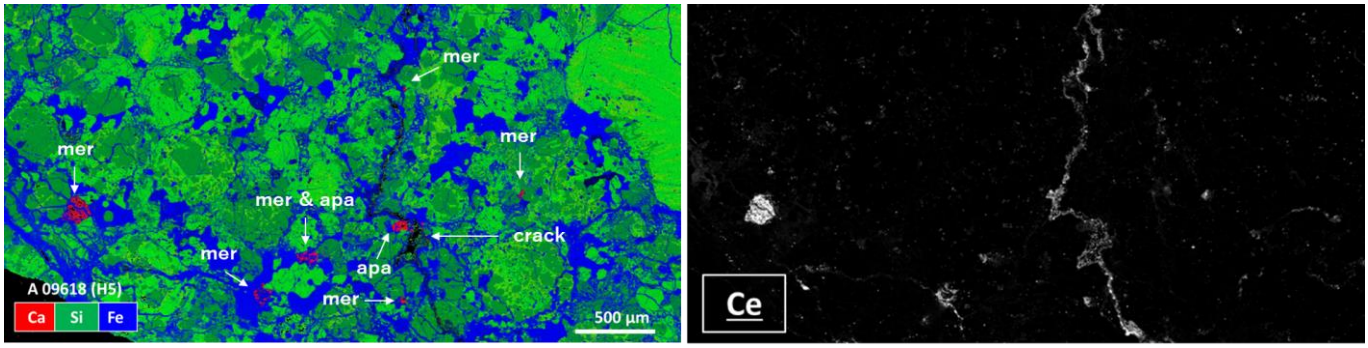

Fig. 1. Elemental maps of Asuka 09618 (H5, WI: C) obtained using LA-ICP-TOF-MS: a combined RGB map (Red=Ca; Green=Si; Blue=Fe; mer: merrillite; apa: apatite) at left; a Ce map at right.

accompanied by a low P_2O_5/SiO_2 in Fig. 2. However, crack-3 displays REE, Th, and U abundances as high as those in crack-1 and crack-2 with a small negative Ce anomaly, even though the P_2O_5/SiO_2 is as low as that observed for crack-4 (Fig. 2). This cannot be explained by the nugget effect of Ca-phosphates. Thus, cracks appear to accumulate unbonded REEs locally as the trace element maps suggest such depositions. Probably, Th and U can deposit in these cracks as well. This is consistent with chemical leaching experiments [*e.g.*, 5], in which REEs, Th, and U have been expected to be deposited in cracks and grain boundaries. The trace element mapping using LA-ICP-TOF-MS reported on here represents the first instance in which such depositions are visually confirmed.

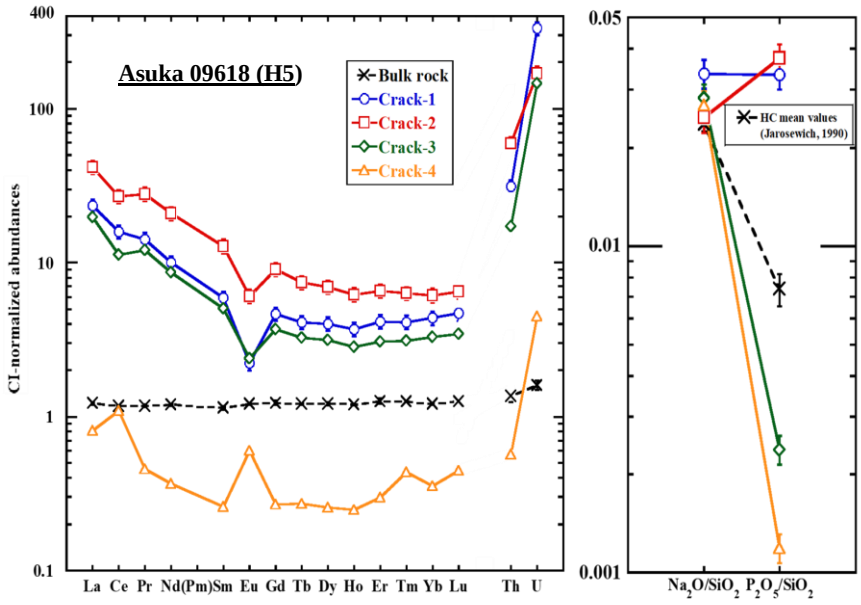

Fig. 2. CI-normalized REE, Th, and U abundances and ratios of Na_2O to SiO_2 and P_2O_5 to SiO_2 in cracks for Asuka 09618 (H5, WI: C). Bulk rock values are from [2]. The Na_2O/SiO_2 and P_2O_5/SiO_2 for bulk rock are calculated from HC mean values in [3]. CI values are from [4].

Based on the LA-ICP-MS line scans, cracks in all of the weathered samples categorized as B/C, C, W1, and W2 in this study display positive Ce anomalies similar to that observed for crack-4 in A 09618 (Fig. 2). A crack having unbonded REEs with a small negative Ce anomaly such as crack-3 in A 09618 is also found in Sahara 97035. The crack also desplays no feature of high P and Ca abundances. Because the positive Ce anomalies and unbonded REE depositions occur in all weathered samples, the pattern observed likely results from terrestrial weathering. According to Mittlefehldt and Lindstrom [6], melting of ice can trigger sample alteration following chemical leaching as demonstrated by the loss of Ca-phosphates in eucrites from Antarctic samples, in line with our observations for cracks in chondrites. Rain or humidity is known to trigger a similar mechanism in hot deserts. During the residence of meteorites in Antarctica or hot deserts, fluids such as melting ice or rain pass through the interior of a meteorite following any physical cracks or grain boundaries. During the passing of such fluids, a fraction of the Ca-phosphates is dissolved or partially dissolved in this fluid. In the case that the Ca-phosphates are completely dissolved, P and Ca completely pass through the meteorite, while REEs largely remain in cracks because REEs are significantly more immobile than P and Ca [7, 8]. At a later stage of this alteration sequence, only Ce remains in the cracks, while the other REEs are removed because Ce is considerably more immobile than the other REEs as a result of oxidation from Ce^{3+} to Ce^{4+} [6]. This is supported by the observation that unbonded REEs deposited in cracks show a negative Ce anomaly. In the case that Ca-phosphates were partially dissolved, it is assumed that only trace elements such as REEs are extracted from Ca-phosphates as a result of an interruption in the ionic bonding between cations, particularly impurity cations, and $(PO_4)^{2-}$ in the Ca-phosphates [2]. Then, in a similar manner, the REEs are mobilized from the cracks while only Ce remains there in the later stages. In hot deserts, such a chemical leaching may occur with secondary carbonates as well as Ca-phosphates. Both alteration scenarios can explain a deposition of unbonded REEs with a small negative Ce anomaly and a depleted REE pattern with a positive Ce anomaly in cracks. The depositions of unbonded REE likely represent a transitional stage of the alteration and the positive Ce anomalies represent a later stage, and as such, positive Ce anomalies may be a common feature in cracks. This is indeed consistent with the observation that only two cracks show a deposition of unbonded REE, while ~20 out of the 51 cracks studied here exhibit a positive Ce anomaly. Therefore, it seems that the depositions of unbonded REE and positive Ce anomalies in cracks are both caused by terrestrial alteration following chemical leaching. However, because bulk elemental abundances including REEs in these samples except for A 09516 are in good agreement with HC mean values [2], this alteration occurs locally only and the effect on the bulk composition is generally limited.

References

[1] Pourkhorsandi *et al*. (2021) *Chem. Geol.* **562**, 120056. [2] Maeda *et al*. (2021) *GCA* **305**, 106-129. [3] Jarosewich (1990) *Meteoritics* **25 (4)**, 323-337. [4] Anders and Grevesse (1989) *GCA* **53**, 197-214. [5] Ebihara and Honda (1984) *Meteoritics* **19 (2)**, 69-77. [6] Mittlefehldt and Lindstrom (1991) *GCA* **55**, 77-87. [7] Middelburg *et al*. (1988) *Chem. Geol.* **68**, 253-273. [8] Bland *et al*. (2006) In *Meteorites and the Early Solar System II* (eds. Lauretta D. S. and McSween Jr. H. Y.), pp. 853–867.

Thermal and shock history of diogenites based on the occurrence of silica minerals

Rei Kanemaru[1], Akira Yamaguchi[2, 3], Naoya Imae[2,3] and Atsushi Takenouchi[4]
[1]*Institute of Space and Astronautical Science,* [2]*National Institute of Polar Research,*
[3]*Graduate University of Advanced Studies, SOKENDAI,* [4]*Kyoto University*

Introduction

Diogenites are a group of HED (howardites, eucrites, diogenites) meteorites [1, 2]. The HED meteorites are considered to have originated from the lower crustal material of asteroid Vesta (e.g., [3]). The petrographic study of HED meteorites provides us the information about thermal and shock history on the HED parent body. Recently, silica minerals in eucrites have been used as an indicator of the thermal and shock history of eucrites (e.g., [4, 5]). However, the occurrence and combination of silica minerals in diogenites have not been well-studied (e.g., [6]). In this study, we investigated the occurrences and compositions of silica minerals in diogenites to better understand the origin. Moreover, on the basis of the observations, we aim to understand the shock and thermal history of diogenites.

Sample and methods

In this study, we studied nine Antarctic and non-Antarctic diogenites. We studied three types of diogenite including unbrecciated diogenites (NWA 7831, NWA 8043, NWA8107), brecciated diogenites (NWA 4965, NWA 8703, Bilanga), and recrystallized diogenites (Tatahouine, Y 002875, Y-74013). These diogenites were observed by an optical microscope and a field emission scanning electron microscope (FE-SEM: JEOL JSM-7100) with an energy dispersive spectrometer (EDS) (Oxford AZtec Energy) and a cathodoluminescence system (GATAN ChromaCL) at the National Institute of Polar Research, Tokyo (NIPR). Silica polymorphs were identified by a Raman spectrometer (Renishow) at NIPR.

Results

We found silica minerals in all studied diogenites (<~1 vol.%). We identified (monoclinic: MC-, pseudo orthorhombic: PO-) tridymite, cristobalite, and quartz in diogenites (Table 1, Fig. 1). These silica minerals mainly occur as short-veins or tiny rounded grains. The combinations of silica minerals in each diogenite were closely related to the types of diogenites. The unbrecciated diogenites (e.g., NWA 7831) show a sharp optical extinction (<~2º) under the optical microscope. These diogenites contain MC tridymite coexisted with a small amount of cristobalite. The brecciated diogenites show undulatory extinction. NWA 8703 shows a weak undulatory extinction (~5º), containing MC tridymite, PO tridymite, and quartz. Bilanga and NWA 4965 show a strong undulatory extinction (~15º), containing only quartz. The recrystallized diogenites show a sharp optical extinction (<~2º). Y 002875 contains MC tridymite and PO tridymite. Tatahouine and Y-74013,1 contain MC tridymite, PO tridymite, and cristobalite.

Discussion

Cristobalite is considered to be a primary silica phase crystallized from diogenitic magma. The cristobalite underwent a phase transition to tridymite during the cooling process. The presence of cristobalite indicates that the diogenites are unequibrium state at the subsolidus temperature. It is suggested that some diogenites experience a rapid cooling process comparable to basaltic eucrites [4]. The modal abundances of quartz in diogenites tend to increase to undulatory extinction angle ranges (~5º to ~15º). In eucrites, it is observed that tridymite transforms silica glass and quartz by shock metamorphism (shock pressure > ~10 GPa) [5]. Thus, quartz in shocked diogenites also transforms from tridymite or silica glass. On the other hand, we could not find quartz in the recrystallized diogenites. The absence of quartz could be due to the difference in pressure and thermal conditions at the shock event. We suggest that recrystallized diogenites experienced strong thermal metamorphism at least stable condition of quartz (>~870 ℃) during shock metamorphism. PO tridymite is observed in brecciated diogenites and recrystallized diogenites. The relationship between PO tridymite and shocked diogenites could be explained by shock pressure and thermal metamorphism. However, the phase transition process of PO tridymite is complex, and we could not constrain the temperature and pressure conditions.

In summary, unbrecciated diogenites retain the primary silica minerals of cristobalite and MC tridymite. On the other hand, brecciated diogenites contain quartz and PO tridymite. It was suggested that these silica minerals were formed by shock metamorphism. In addition, the amount of quartz increased with the increase of shock metamorphism. Recrystallized diogenites contain MC tridymite, PO tridymite, and cristobalite. The absence of quartz indicates that the recrystallized diogenite experienced stronger thermal metamorphism than brecciated diogenites.

Table 1. Silica minerals in studied diogenites

Samples	Texture			Silica minerals			
		Undulatory extinction	Shock vein	Crs	PO Trd	MC Trd	Qtz
NWA 7831	unbrecciated	<2º (Sharp)	-	Yes		Yes	
NWA 8043	unbrecciated	<2º (Sharp)	-	Yes		Yes	
NWA 8107	unbrecciated	<2º (Sharp)	-			Yes	
NWA 8703	breccia	~5º (Weak)	-		Yes	Yes	Yes
NWA 4965	breccia	~15º (Strong)	-				Yes
Bilanga	breccia	~15º (Strong)	Yes?				Yes
Tatahouine	Recrystallized	<2º (Sharp)	-	Yes	Yes	Yes	
Y-002875	Recrystallized	<2º (Sharp)	-		Yes	Yes	
Y-74013,1	Recrystallized	<2º (Sharp)	-	Yes	Yes	Yes	

Crs: Cristobalite; PO Trd: Pseudo orthorhombic tridymite; MC Trd: Monoclinic tridymite; Qtz: Quartz.

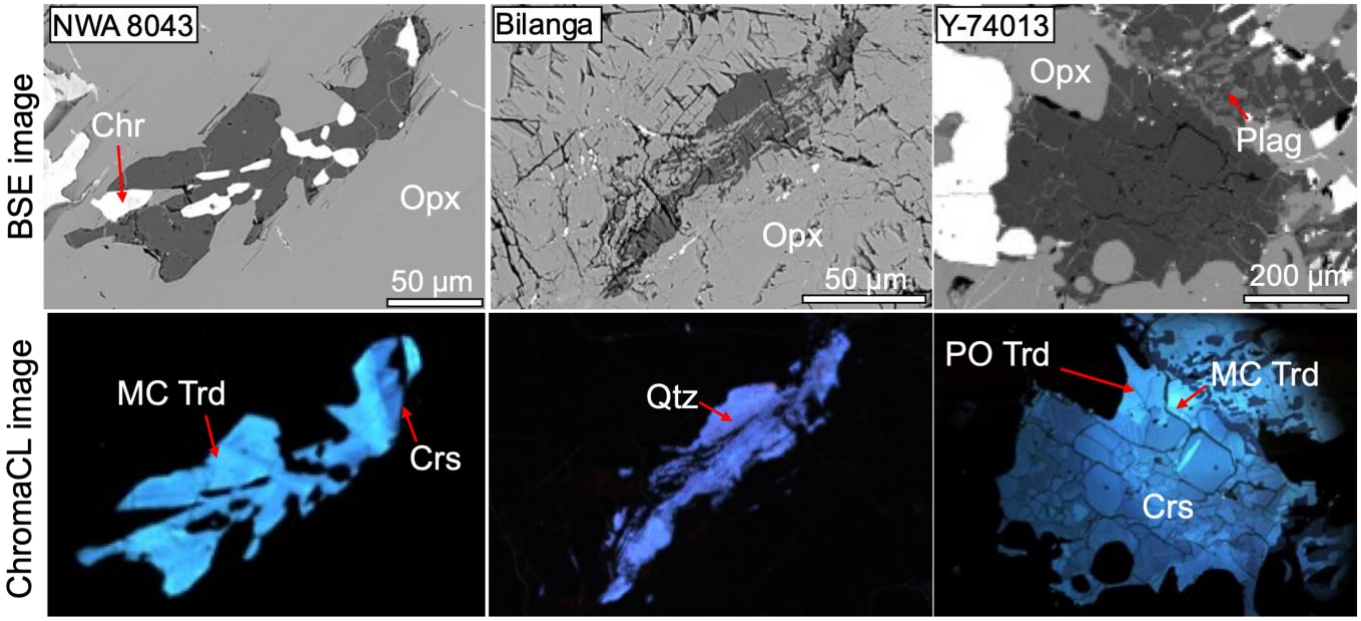

Fig. 1. BSE and chromaCL images of silica minerals in diogenites. MC tridymite shows a bright aqua-blue CL emission. Cristobalite and PO tridymite show a dark blue CL emission. Quartz shows a dark purple CL emission.

References

[1] Takeda, H., Mori, H., Prinz, J. s., Harlow, G. E., Ishii, T., 1983. Mineralogical comparison of Antarctic and non-Antarctic HED howardites–eucrites–diogenites. *Proc. Symp. Antarct. Meteorites.* 8, 114-116.

[2] Yamaguchi, A., Barrat. J. A., Greenwood, R., 2017. Achondrites. *Springer*.

[3] Binzel, R.P., Xu, S., 1993. Chips off asteroid 4 Vesta: evidence for the parent body of basaltic achondrite meteorites. *Science.* 260, 186–191.

[4] Ono, H., 2020. Crustal evolution of asteroid Vesta as inferred from silica polymorphs in eucrites. Doctoral Dissertation, Department of Earth and Planetary Science, Graduate School of Science, The University of Tokyo.

[5] Kanemaru, R., Yamaguchi, A., Imae, N., Takenouchi. A., Nishido, H., 2021. Shock effects in silica minerals in eucrites. JPGU 2021, PPS07-14.

[6] Benzerara, K., Guyot, F., Barrat, J. A., Gillet, P., Lesourd, M., 2002. Cristobalite inclusions in the Tatahouine achondrite: Implications for shock conditions. *Amer. Miner.*, 87, 1250-1256.

Determination of the real size distribution of chondrules based on the measured size distributions in thin sections

József Vanyó[1], Arnold Gucsik[1, 2], Árpád Csámer[2], Péter Futó[2], and János Sztakovics[1]

[1]*Eszterházy Károly Catholic University, Faculty of Natural Sciences, Institute of Chemistry and Physics, Department of Physics, H-3300, Eger, Leányka utca 6-8*

[2]*University of Debrecen, Cosmochemistry Research Group, Department of Mineralogy and Geology, Institute for Earth Sciences, University of Debrecen, H-4032, Egyetem tér 1 Debrecen, Hungary*

The conditions under which chondrules are formed can be inferred mainly from their physical, chemical and geometric properties. So far, chemical properties have been studied in numerous studies, but little attention has been focused on geometric characteristics, more specifically size distributions. However, the formation conditions of chondrues may also be closely related to these propoerties above.

In the articles published so far on this topic, the characterization of geometric properties was almost exclusively limited to the two-dimensional size distribution of the plane sections of the spheres, measured by thin sections. However, these two-dimensional size distributions do not match the true particle size distribution of the chondrules, and thus the previous flat section size distributions are not directly suitable for drawing correct conclusions about the conditions under which they were formed. The significance of the real particle size distributions may be further enhanced by the fact that, knowing these, it is likely that further classification of meteorites would be possible.

In the course of this research, our first goal was to find a relationship between the two-dimensional distributions of the sections and the real particle size distribution of the chondrules. The question arises naturally as to whether it is possible to use this relationship to develop a procedure to determine the true particle size distribution of the concentrates from the two-dimensional distributions. Since the preparation of thin grinds produces flat sections of the original condonants, the problem is essentially how to restore the real particle size distribution of the original spheres from a distribution made with the help of a two-dimensional section.

The problem seems impossible at first hearing, since at pruning we in some sense "lose one dimension". If the diameter of a chondrule is measured on the thin section, it can only be stated that the original diameter of the chondrule is surely greater than or equal to this, but we cannot determine the original true size. Therefore, for some chondrules, the true size cannot be determined from the size obtained during the section. However, this is not the case with distributions. Using a plausible hypothesis, the relationship between the distributions can be written on the lost dimension, and thus, surprisingly in the light of the above problem, the final question is answered positively, the original particle size distribution can be determined from the distribution of thin sections.

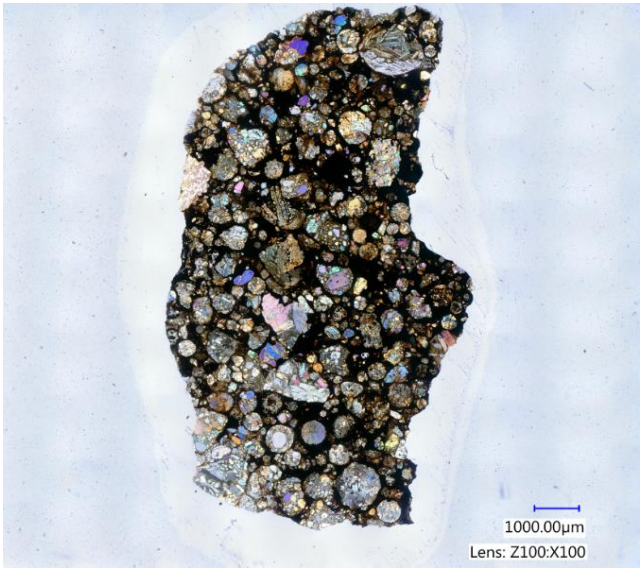

Figure 1. A recording of a studied plane section.

The problem is fundamentally statistical and, as we will see, leads to the field of probability calculation, so that our answer cannot be without the use of the tools of higher mathematics. We tested our results using Monte-Carlo simulations and found a perfect match between mathematical calculations and simulation results.

We intend to continue our research in several directions. One direction is to measure the distributions for as many thin sections as possible and to determine the true particle size distributions from them. A recording of such a plane section is shown in Figure 1.

Scientists in the fields of meteorite study do not always possess the advanced mathematics necessary to understand numeracy, so as a continuation of the research, another goal in the future is to create an application that can determine the real particle size distribution based on the measured distribution.

Multiscale characterization of the Asuka 12169 meteorite – rehearsal of Hayabusa2 returned sample analysis –

M. Uesugi[1], M. Ito[2], N. Tomioka[2], N. Imae[3], A. Yamaguchi[3], M. Kimura[3], N. Shirai[4], T. Ohigashi[5], M-C. Liu[6], R.C Greenwood[7], K. Uesugi[1], A. Nakato[8], K. Yogata[8], H. Yuzawa[5], Y. Kodama[9,*], M. Yasutake[1], K. Hirahara[11], A. Takeuchi[1], I. Sakurai[12], I. Okada[12], Y. Karouji[8], T. Yada[8] and M. Abe[8]

*[1]JASRI/SPring-8, [2]JAMSTEC Kochi, [3]NIPR, [4]Tokyo Met. Univ., [5]UVSOR/IMS, [6]UCLA, [7]Open Univ.,[8]JAXA-ISAS, [9]MWJ, [11]Osaka Univ., [12]Nagoya Univ., *Toyo Corp.*

Introduction

Regolith particles of the asteroid Ryugu were distributed to the initial analysis teams and the Phase2 curation teams in mid 2021. The sample are free from terrestrial contaminations, and not exposed to the terrestrial atmosphere. In order to maximize the scientific gain from the samples, we must (?) keep such high-level cleanness of the sample against the terrestrial materials, throughout the analysis as long as possible. Prior to the analysis of the Hayabusa2 returned samples, the Phase2 curation Kochi team [1] conducted rehearsal analysis of a mm-sized fragment of Antarctic meteorite, Asuka (A) 12169 CM3.0, by a series of multibeam micro analytical techniques prepared in each institute. The analytical flow starts from non-destructive method such as a synchrotron radiation computed tomography (SR-CT) and SR x-ray diffraction (SR-XRD), to destructive but high-resolution method such as scanning transmitted x-ray microscopy and near edge x-ray absorption fine structure (STXM-NEXAFS), nano-scale secondary ion mass spectrometry (NanoSIMS) and transmission electron microscopy (TEM). We focus on the characteristics of organic materials in aspect of relation to the structure and chemical composition of surrounding minerals. Because A 12169 experienced only minimal aqueous alteration [2], organic materials in A 12169 would be pristine compared to those of other meteorites. The study would help us for a better understanding of the evolution of organic material in Ryugu samples.

Experiments

A small fragment of A 12169, 1mm x 1mm x 2mm, was examined by SR-CT with voxel size around 3 μm for the bulk 3D texture, and by SR-XRD for the bulk mineralogy. After the SR analysis, the sample was cut by a diamond wire saw without using glue or wax as well as lubricants, to prevent contamination. Three ultrathin sections were picked up from the matrix portions of the cut surface using focused ion beam (FIB). The thin sections were investigated by STXM-NEXAFS, TEM, and NanoSIMS to analyze organic materials.

Results

Figure 1 shows the STXM-NEXAFS images of A 12169, a part of the sequential analysis. Organic globules in A 12169, appear as spots of carbon enriched regions in map of carbon concentration in Fig. 1, were abundant compared to other CM chondrites. Some organic globules show a hollow structure, which is well known as hollow-organic nano globule [e.g. 3-5]. Note that region 1 in Fig. 1 shows two distinct areas with different carbon concentrations. TEM analysis revealed that low carbon region consist mainly of tochilinite-cronstedtite intergrowth (TCI). C-NEXAFS map also shows relatively high abundance of carbonates in low carbon region than high carbon region.

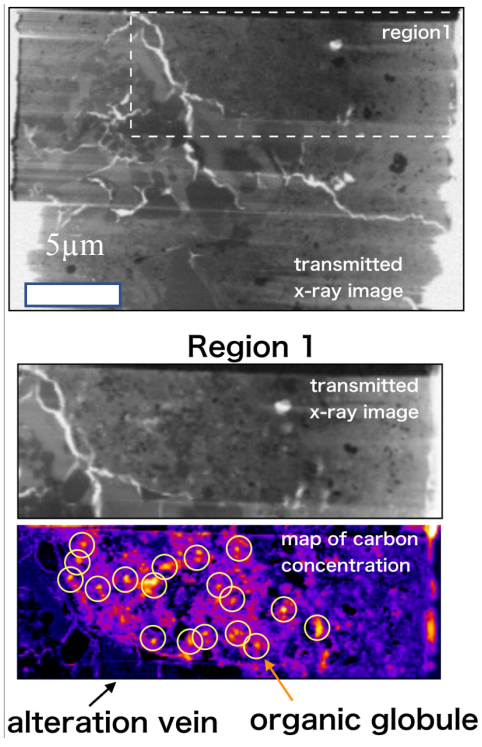

Figure 1. STXM-NEXAFS image of A 12169. Upper: transmitted x-ray image of whole thin section, middle: enlarged view of region 1 in top image, Bottom: carbon concentration image obtained by C-NEXAFS. Bright spots indicated by yellow circles show organic globules. Lower left part of image is depleted in carbon (alteration vein).

Discussion

The low carbon region would be a part of a vein which had been formed by aqueous alteration, because of its high abundance of hydrous minerals. Organic globules were almost absent inside the alteration vein. The result indicates that the organic globules in high carbon region may be formed in interplanetary and/or interstellar region prior to the aqueous alteration in the parent body of A 12169, and were not robust against the aqueous alteration.

References

[1] Ito M. et al. (2020) Hayabusa Symp. [2] Kimura M. et al. (2020) Polar Sci. 26:100565. [3] Garvie L. A. J. and Buseck P. R., (2006) MAPS 41:633. [4] Nakamura K. et al. (2006) Science, 314:1439. [5] De Gregorio B.T. et al. (2013), MAPS 48:904.

Characterizing the Ryugu samples using the laboratory-based XRD and the meteorite collections at NIPR

N. Imae[1], A. Yamaguchi[1], M. Kimura[1], M. Ito[2], N. Tomioka[2], M. Uesugi[3], N. Shirai[4], T. Ohigashi[5], M-C. Liu[6], R.C. Greenwood[7], K. Uesugi[3], A. Nakato[8], K. Yogata[8], H. Yuzawa[5], Y. Kodama[9,*], M. Yasutake[3], K. Hirahara[10], A. Takeuchi[3], I. Sakurai[11], I. Okada[11], Y. Karouji[8], T. Yada[8] and M. Abe[8]

[1]NIPR, [2]JAMSTEC Kochi, [3]JASRI/SPring-8, [4]Tokyo Met. Univ., [5]UVSOR/IMS, [6]UCLA, [7]Open Univ., [8]JAXA-ISAS, [9]MWJ, [*]Toyo Corp., [10]Osaka Univ., [11]Nagoya Univ.

Introduction

The laboratory-based X-ray diffraction is a useful technique for characterizing stony meteorites via whole powder pattern fitting [e.g., 1–3] and μXRD [e.g., 4]. We have also shown that this method is useful for the classification of ordinary chondrites [5], shock effects of ordinary chondrites and eucrites [e.g., 6–7], thermal metamorphism of CO3 [8], and hydrous alteration of CM2 [9]. The relative intensity ratio (RIR) method was used, and polished thin sections with large surface areas, more than 1 cm^2 were typically used. In the present study, we examined hydrous altered carbonaceous chondrites using the technique applicable to limited volumes, small surface area polished sections (several mm^2) and ~0.5–10 mg fragments toward the application to Ryugu. This report is part of the ongoing Phase2 Kochi advanced curation studies of returned Hayabusa 2 samples.

Experiments

We chose carbonaceous chondrites, CM (Y-791198, Y-793321, Y-82042, A-881655, A 12437, Jbilet Winselwan, Murchison), CY (B-7904, Y-82162, Y-86029, Y-86720, Y-86737, Y-86789, Y 980115, Y 980134), CI (Orgueil), CO3 (ALH-77307, A-881632), and C ung (Tagish Lake) for the present study. For each chondrite we prepared the following: a dry polished mount embedded in epoxy resin and/or in sulfur, 0.5–6 mg powder in a non-reflection silicon plate (5 mm in diameter and 0.2 mm in depth, surface area 0.2 cm^2) as well as a glass plate, and/or ~1–10 mg fragment on carbon nanotube (CNT) [10]. The Cu Kα X-ray beam (40 kV and 40 mA) of the X-ray diffractometer (SmartLab, RIGAKU) was broad, Bragg and Brentano (BB) method, or focused by a polycapillary unit (CBO-f unit), both in-plane rotation around the sample-area center, 20 rpm or larger. The acquisition time was approximately 8 hours for BB and 40 hours for CBO-f, the 2θ range was up to 80º for BB and 50º for CBO-f. Two techniques were used for preparing powdered samples: (1) only ~0.5-5 mg sample was pressed using a sapphire glass plate on the silicon non-reflection silicon plate with the Miller index of (105), and (2) agate mortar and agate pestle for sample mass of ≥~0.1 g was used. As well as small and limited samples, standard polished thin sections of Y-86720 (74-1; 76 mm^2), Y 980115 (,70-1; 98 mm^2), B-7904 (,60-1; 144 mm^2), ALH-77307 (,85-1; 50 mm^2), A-881632 (,51-6; 100 mm^2), Y-791198 (,61-3; 70 mm^2), Murchison (469 mm^2), and Jbilet Winselwan (19 mm^2) were also studied similarly for reference purposes.

Results

Diffractions from the epoxy resin of small samples (surface area with sub cm^2) for both BB and CBO-f methods are not intense. Many sulfur peaks from sulfur-embedded polished samples are observed and are necessary to be distinguished with peaks from the measured sample. Any fragment (~1–10 mg) on CNT normally shows the consistent diffraction pattern from powder, but needs time and has a high background. The entire filling powder (~5–10 mg) by the non-reflection silicon plate gives higher intensity, and the background is minimal. Then, a very similar diffraction pattern to Y-82162 (CY with the heating stage II-III, [11]) was observed for Y-86029, Y-86737, Y 980115, and Y 980134, suggesting a pairing with ~5 mg powder. The method was also applied to partially filling powder of Orgueil, ~0.5–1 mg, which generally showed a very similar pattern to the entire filling case.

Discussion

Due to the limited amount of sample material that is available for study, 1 mg or less, then analysis using the non-reflection silicon plate technique is more suitable than employing a CNT. Because the more intense and higher angular-resolution diffraction from powders is obtained. The press method of a tiny sample by sapphire glass on the non-reflection silicon plate is suitable for the Ryugu analysis by the present powder method.

References

[1] Dunn T. L. et al. (2010) M&PS 45:123. [2] Howard K. T. et al. (2011) GCA 75:2735. [3] King A. J. et al. (2021) GCA 298:167. [4] Jenkins L. E. et al. (2019) M&PS 54:902. [5] Imae N. et al. (2019) M&PS 54:919. [6] Kanemaru R. et al. (2020). Pol. Sci. 26:100605. [7] Imae N. and Kimura M. (2021) Am. Min. 106:1470. [8] Imae N. and Nakamuta Y. (2018) M&PS 53:232. [9] Imae N. and Kimura M. (2020) 11th Symp. on Pol. Sci. [10] Uesugi M. et al. Rev. Sci. Instrum. 91:035107. [11] Nakamura T. (2005) JMPS 100:260.

What is type 3.0 of chondrites?

Makoto Kimura
National Institute of Polar Research

Chondrites are classified into petrologic types 1-6. Among them, type 3 chondrites almost escaped thermal metamorphism and aqueous alteration. Type 3 chondrites are classified into 3.0 to 3.9 [e.g., 1], reflecting thermal metamorphic degree. Type 3.0 chondrites are further divided into 3.00 to 3.05 [2]. They are the most primitive chondrites to preserve the characteristic features of the constituent materials before the secondary processes in their parent bodies [e.g., 3]. However, the classifications of some chondrites that experienced relatively low degrees of thermal metamorphism and aqueous alteration are often problematic, for example, how to classify them and how to distinguish between types 3.0 and 2.9. Therefore, here I reconsider the classification criteria of type 3.0. I also discuss the distribution of this type in chondrite groups. Here I include types 3.00 to 3.05 into 3.0 together.

Type 3 chondrites are characterized by heterogeneous chemical compositions of silicate minerals and the preservation of primitive texture, such as well-defined chondrules and the occurrence of opaque matrix. In addition, type 3.0 chondrites show the following characteristic features to distinguish it from types 3.1-3.9: Cr distribution in ferroan olivine, the thermoluminescence and cathodoluminescence features, the abundance of presolar grains, the occurrence of hydrated phases especially in the matrix, and minor element contents in Fe-Ni metal [e.g., 2, 4]. Type 3.0 ordinary chondrites are also characterized by the occurrence of nearly pure chromite [5]. All type 3.0 chondrites seem to contain amorphous materials in the matrix [e.g., 6], although some altered chondrites also have it.

Recent studies showed that type 3.0 ordinary and carbonaceous chondrites also have other distinct features; Plagioclase in them contains [ ]Si_4O_8 component and high MgO content [e.g., 7]. Fe-Ni metal shows the positive Ni-Co correlation approximately along with the solar abundance. It abundantly contains some minor elements, such as Si, P, and Cr [8]. Since these features are not noticed in chondrites greater than or equal to type 3.1, they can be used to classify type 3.0 chondrites, in addition to the criteria mentioned above.

The problem is how to distinguish type 3.0 and less than 2.9 with aqueous alteration features. Although type 3.0 chondrites are hardly subjected to the secondary processes, all known such chondrites contain hydrous phases [e.g., 9]. If we define type 3.0 to escape the alteraion completely, all known type 3.0 chondrite must be reclassified into not greater than 2.9. Since we need to avoid such confusion, I propose the new criteria for type 3.0; Silicate, oxide, metal, and sulfide minerals do not show the alteration features under optical microscope and SEM observations. Melilite and anorthite in refractory inclusions and chondrules, quickly altered phases, do not show the aqueous alteration features in type 3.0 chondrites. On the other hand, glass in chondrule and amorphous material in the matrix are partially, but never totally, hydrated in these chondrites. These phases are the most susceptible to alteration. These classification criteria are consistent with those for not only CO and ordinary chondrites but the recent classification of CR3.0 [10] and CM3.0 [11] chondrites. Abundant O-rich presolar grains in these carbonaceous chondrites also support such criteria [12].

Although all chondrite groups include type 3 samples, type 3.0 has not been noticed in all kinds of chondrite. So far, type 3.0 is recognized from H, L, LL, CM, CO, CR, and Acfer 094. In the other chondrites, such as CV and E chondrites, no type 3.0 has been reported. Although we can not exclude the possibility of sampling problem, we already have abundant samples for these chondrite groups without type 3.0 from Antarctica and other areas. Therefore, I suggest that such a heterogeneous distribution of type 3.0 reflects the degree of the secondary parent body process, such as thermal and/or shock metamorphism.

References

[1] Sears D. W. G. et al. 1991. Proc. Lunar and Planetary Science 21: 493-512. [2] Grossman J. N. and Brearley A. J. 2005. Meteoritics & Planetary Science 40: 87-122. [3] Brearley A.J. 2017. 8h Symposium on Polar Science, National Institute of Polar Research, [4] Huss G. R. et al. 2006. Thermal metamorphism in chondrites. In Meteorites and the Early Solar System [5] Kimura M. et al. 2006. Geochimica et Cosmochimica Acta 70: 5634-5650. [6] Dobrică E. and Brearley A. J. 2020. Meteoritics & Planetary Science 55: 649-668. [7] Siron G. et al. 2021. Geochimica et Cosmochimica Acta 293: 103-126. [8] Kimura M. et al. 2008. Meteoritics and Planetary Science 43: 1161-1177. [9] Davidson J. et al. 2019. Geochimica et Cosmochimica Acta 265: 259-278. [10] Harju E. R. et al. 2014. Geochimica et Cosmochimica Acta 139: 267-292. [11] Kimura M. et al. 2020. Polar Science 26: 100565. [12] Xu Y. et al. 2020. 11th Symposium on Polar Science, National Institute of Polar Research.

Chemical analyses of Fe – rich chondrule phases in Kaba (CV3) carbonaceous - chondrite. Implications on the bulk elemental composition of terrestrial planetary cores.

P. Futó[1] and A. Gucsik[2]
[1]*University of Debrecen, Cosmochemical Research Group, Department of Mineralogy and Geology, Debrecen, Egyetem tér 1. H-4032, Hungary (dvision@citromail.hu)*
[2]*Eszterházy Károly Catholic University, Faculty of Natural Sciences, Institute of Chemistry and Physics, Department of Physics, H-3300, Eger, Leányka utca 6-8.*

Most chondrules in chondrites are dominated by olivine, pyroxene, and feldspar. They may also include metal alloys, sulfides, nitrides, phosphides in varying proportions, which highlight to their formation in diverse physical and chemical environments (Hazen et al. 2021). Different metallic phases can be found in the mineral assemblages of chondrules. The metallic phases may be Ni – rich metal (kamacite), moreover, troilite (FeS) and pentlandite $(Fe, Ni)_9S_8$, which belong to the most common iron – nickel sulfides in chondrites.
We have performed several laboratory analyses to study metallic alloys in different mineral constituents of Kaba meteorite, which is the one of the most primitive C – chondrite (Krot et al. 1998). Kaba contains Fe – rich chondrule phases representing several characteristic mineral species in the Bali-type $CV3_{OxB}$ chondritic material.

Analytical experiments: According to Gucsik et al. (2013) quantitative analyses for minor and major elements in olivine were obtained by wavelength-dispersive spectrometry (WDS) linked to a JEOL JXA-8900R SEM at Okayama University of Science (Okayama, Japan). Operational conditions were: accelerating voltage of 15 kV and a probe current of 40 nA on a Faraday cup equipped with PCD (probe current detector), using a focused beam. The ZAF program installed in the workstation was employed for matrix corrections. The detection limit for quantitative analysis (WDS) ranged between 0.03 (light elements) and 0.04 (heavy elements) wt%, and was around 0.005 wt% for the qualitative measurements by EDS. The Secondary Electron Image (SEI) and backscattered electron (BSE) images were captured by JSM-5410LV SEM.

Results: Three Fe – rich chondrule mineral phases have been indentified in Kaba. We have found that S, Ni and Co have the higher relative abundance in the examined Fe-rich mineral phases of the chondrules in the Kaba c-chondrite (Table 1.).

FeO		**Pentlandite**			**Kamacite**		
			wt%	mol%		wt%	mol%
FeO	97.63	S	34.48	48.23	Fe	92.33	89.43
Na_2O	0.52	Fe	44.76	35.94	Ni	4.67	4.3
MgO	0.28	Ni	19.45	14.86	Co	0.62	0.57
Cr_2O_3	0.51	Co	1.18	0.9	Mg	0.15	0.33
	98.94	Si	0.14	0.22	Si	0.17	0.33
			100.01	100.15		97.94	94.96

Table 1. mineral Fe-rich phases (FeO , pentlandite) (Fig.1) and Fe-Ni metal (kamacite) (Fig.2) in chondrules.

Conclusion: Although, CCs have not been derived from the central region of their parent bodies, the chemical composition of their metallic mineral components in the primitive carbonaceous chondrite is similar to the iron – bearing meteorites. Thus, the complex mineralogy of c – chondrites with compositionally varying metallic phases implies on the characteristic bulk elemental composition of the Fe - dominated metallic cores (with relatively high S, Ni and Co abundances) of chondrite parent asteroids and more massive planetary bodies in the Solar System.

Acknowledgements - Authors express thanks to Taro Endo for his help by providing experimental data.

References

Gucsik A., Endo T., Nishido H., Ninagawa K., Kayama M., Berczi Sz., Kimura J., Miura H., Gyollai I., Simonia I., Rozsa P., Posta J., Apai D., Mihalyi K., Nagy M., Ott U. Cathodoluminescence microscopy and spectroscopy of forsterite from Kaba meteorite: An application to the study of hydrothermal alteration of parent body. Meteoritics & Planetary Science, 48. 2577-2596, 2013.
Hazen, R. M., Morrison S. M., Prabhu A. An evolutionary system of mineralogy. Part III: Primary chondrule mineralogy (4566 to 4561 Ma), American Mineralogist, 106, 325 – 350, 2021.

Krot A. N., Petaev M. I., Scott E. R. D., Choi B., Zolensky M. E., Keil K. Progressive alteration in CV3 chondrites: More evidence for asteroidal alteration, Meteoritics & Planetary Science, 33. 1065-1085, 1998.

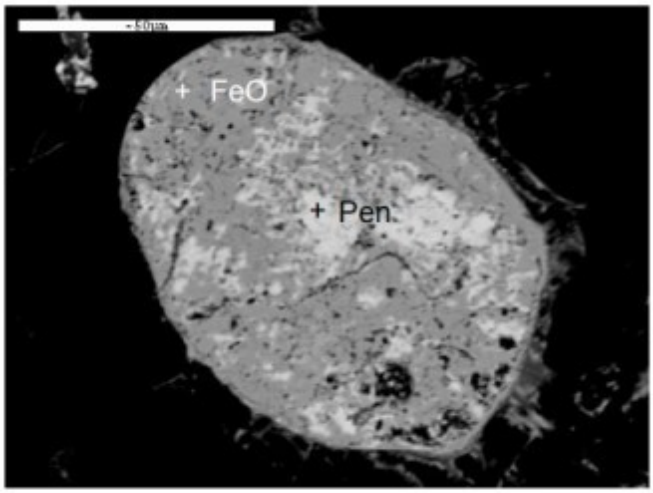

Figure 1. Fe -rich phases in chondrule.

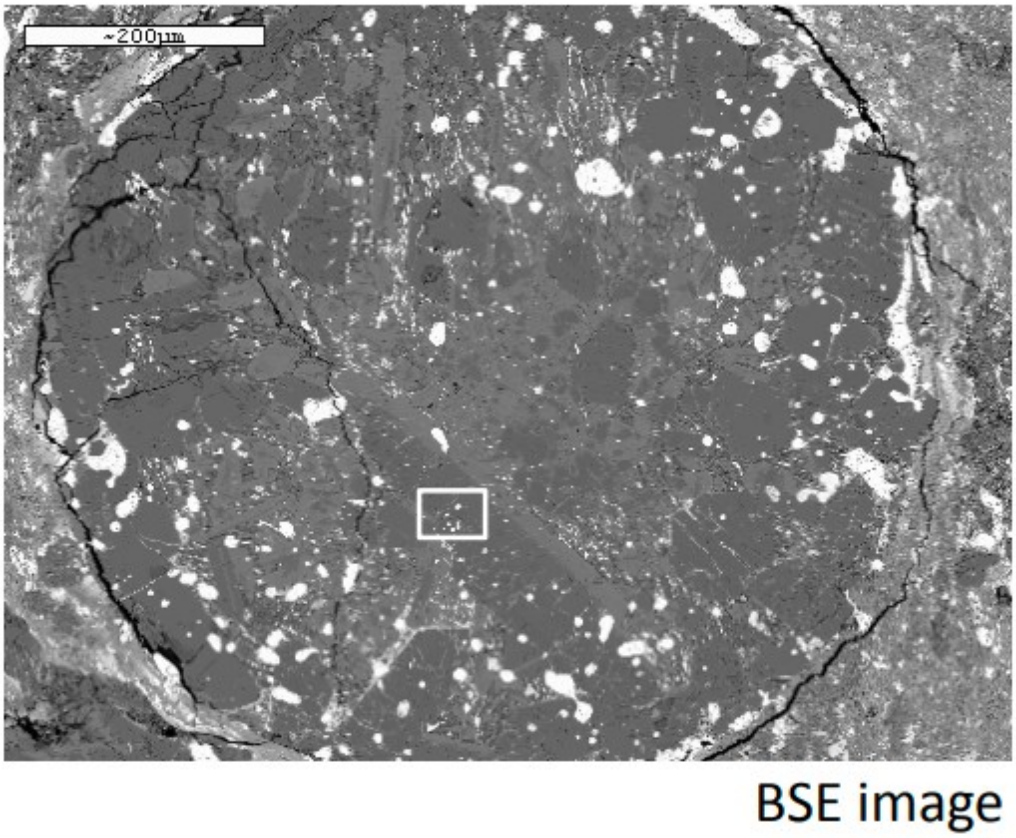

Figure 2. Fe-Ni metal in chondrule.

On the bulk mineralogical composition of carbonaceous chondrites in low-Mg/Si planetary systems.

P. Futó[1] and A. Gucsik[2]
[1]*University of Debrecen, Cosmochemistry Research Group, Department of Mineralogy and Geology, Debrecen, Egyetem tér 1. H-4032, Hungary (dvision@citromail.hu)*
[2]*Eszterházy Károly Catholic University, Faculty of Natural Sciences, Institute of Chemistry and Physics, Department of Physics, H-3300, Eger, Leányka utca 6-8.*

The chemical analyses of chondritic meteorites provides important informations to study the chemical evolution of the Solar-system.
The Mg/Si ratio is the one of the most important elemental ratios, which controls the silicate mineralogy of terrestrial planets.The obervations of stellar element abundances of FGK stars in the Solar neighbourhood show that the largest fraction of them have Mg/Si ratios between 1 and 2 (Delgado Mena et al. 2010). The majority of these stars have higher Mg/Si ratios than the Solar value. At the same time, a smaller fraction of the observed stars exhibit low-Mg/Si ratios, which are smaller than 1.

In the planetary systems, with lower Mg/Si ratio than Solar (Mg/Si=1.05) (Asplund et al. 2005), the mineral constituents of the chondrite components have been formed in a Mg-depleted chemical enviroment. The plausible composition of characteristic mineral components of c-chondrites has been investigated as a function of a decreased Mg/Si molar ratio.
Chondrules are thought to be composed of Mg-rich olivine and pyroxenes, similarly to the mineralogy of c-chondrites with higher Mg/Si ratio. However, the weight percent of pyroxenes has been calculated to be higher in the Mg-poor chondrules than that of the c-chondrites in the Solar System. Pyroxenes in chondrules of Mg-poor chondritic meteorites are consist of a higher amount of high-Ca pyroxenes compared to that of the Mg-rich c-chondrites. Hence, the one of the main mineral component of Mg-poor chondrules is being made up mostly a solid solution between the diopside ($CaMgSi_2O_6$) and hedenbergite ($CaFeSi_2O_6$) endmembers in the high-Ca pyroxene subgroup. Al-rich chondrules contain plagioclase including mostly andesine and oligoclase.
The mineral assemblage of CAIs (calcium-aluminium-rich inclusions) can be depleted in forsterite and anorthite, while it can be richer in gehlenite ($Ca_2Al_2SiO_7$) and diopsidic pyroxenes than chondrites in Solar-system. One group of CAIs may be enriched in grossite ($CaAl_4O_7$) containing the variable abundances of melilite, spinel ($MgAl_2O_4$) and hibonite ($CaAl_{12}O_{19}$).
AOAs (amoeboid olivine aggregates) are thought to have been depleted in forsterite, anorthite and Al-rich diopside. AOAs have been characterized by a volatile- and moderately volatile- depleted elemental composition similarly to the CAIs.
The presented mineral composition of c-chondrites concerns the chondrite parent bodies with bulk Mg/Si values ranging from ~ 0.9-1. The varying degrees of Mg-depletion can yield a majority of diposides in the mantle mineral composition of parent asteroids.

A significant fraction of low-Mg/Si FGK stars in the Solar neighbourhood are thought to host rocky planets, which have Mg-depleted mantle and crustal mineralogy. The variation of Mg/Si ratio can also result in mineral diversity in rocky planetary bodies if their bulk Mg/Si ratios are below 1. In the low-Mg/Si planetary systems, olivines ($(Mg,Fe)_2SiO_4$) and pyroxenes ($(Mg,Fe,Ca)SiO_3$) are also the two most abundant mineral groups in chondritic meteorites. However, the weight percent ratios of their mineral components are different from those of chondrites, which had been formed in higher-Mg/Si planetary systems. The Mg-depleted mantles in the parent asteroids of carbonaceous chondrites are likely to contain higher amount of diopside and Na-pyroxenes (jadeite, aegirine).

References

Asplund, M., Grevesse, N., Sauval, J., The solar chemical composition, Cosmic Abundances as Records of Stellar Evolution and Nucleosynthesis, ASP Conference series, 336, 25. 2005.
Delgado Mena, E., Israelian G., González Hernández J. I., Bond J. C., Santos N. C., Udry S., Mayor M., Chemical clues on the formation of planetary systems: C/O versus Mg/Si for HARPS GTO sample, The Astrophysical Journal, 725, 2349-2358, 2010.

An attempt for estimating aqueous alteration environment from Raman spectra of iron sulfide

Keisuke Narahara[1], Shu-hei Urashima[1], Akira Yamaguchi[2], Naoya Imae[2], and Hiroharu Yui[1]
[1] *Department of Chemistry, Graduate School of Science, Tokyo University of Science*
[2] *National Institute of Polar Research*

[Introduction] Aqueous alteration is one of the most important processes for the chemical evolution in asteroids. Because how chemical reactions proceed is highly dependent on the environment such as temperature and pressure, several researchers have tried to identify them on parent bodies of meteorites, especially for carbonaceous chondrites.[1] However, pH and redox potential of water, which are also important factors to determine the chemical reaction in aqueous solutions at the parent bodies, are not well understood yet. This is because these aqueous parameters are difficult to be estimated from elemental composition, degas profiles, or the presence/absence of specific minerals. We have recently attempted to estimate the aqueous parameters through chemical composition of pyrrhotite. Pyrrhotite is one of iron sulfide minerals described as $Fe_{1-x}S$. The factor "1-x" is continuously variable by the elution of Fe^{2+} to the aqueous solution surrounding it. Because the degree of the elution depends on the pH and redox potential as well as the temperature, we hypothesized that they can be estimated from the chemical composition of pyrrhotite. As a nondestructive and microscopic probe, we focused our attention to Raman spectroscopy because meteorites are generally rare and heterogeneous. In this study, we measured Raman spectra of iron sulfides in Y 980115 as an example of carbonaceous chondrites possessing CI characteristics, i.e. extensively aqueously altered.

[Experimental] A chip of Y 980115 measured was loaned from National Institute of Polar Research. Raman spectra of the terrestrial pyrrhotites, which were collected at (A) Nikolaevskiy mine and (B) Kavalerovo mining district (both in Russia), were also observed as references. Microscopic Raman measurement was performed on Raman-11i (Nanophoton) with an objective lens of Nikon Plan Flour (×40 / NA 0.75, WD 0.66 mm) at 532 nm excitation (5 mW at the sample surface).

[Results and Discussion] Raman spectra obtained from yellowish, luster minerals on Y 980115 are shown in Figure 1a-d. While the spectra in Figure 1a-c are similar to each other, the spectrum in Figure 1d was different from them. The former is assignable to pyrrhotite by the comparison with previously reported spectra of a carbonaceous chondrite LON 94101 (CM2, collected at Lonewolf Nunataks in Antarctica).[2] The latter (in Figure 1d) was assigned to nickel-bearing iron sulfide, pentlandite $(Fe, Ni)_9S_8$, which should be excluded from the analysis. Slight variation of the peak frequency in Figure 1a-c might reflect chemical composition (1-x) of pyrrhotite, but currently it is under debate. Figure 1e-f shows Raman spectra observed for the terrestrial pyrrhotites (A and B). Although the spectrum for the fleshly cleaved surface (A, Figure 1e) was different from those on Y 980115, the spectrum for the long-time air-exposed surface (B, Figure 1f) reproduces them. This indicates that pyrrhotite on Y 980115 was oxidized to some extent. We are planning to compare Y 980115 pyrrhotites with various pyrrhotites which were exposed to different environment for elucidating the aqueous alteration environment of the parent body of Y 980115.

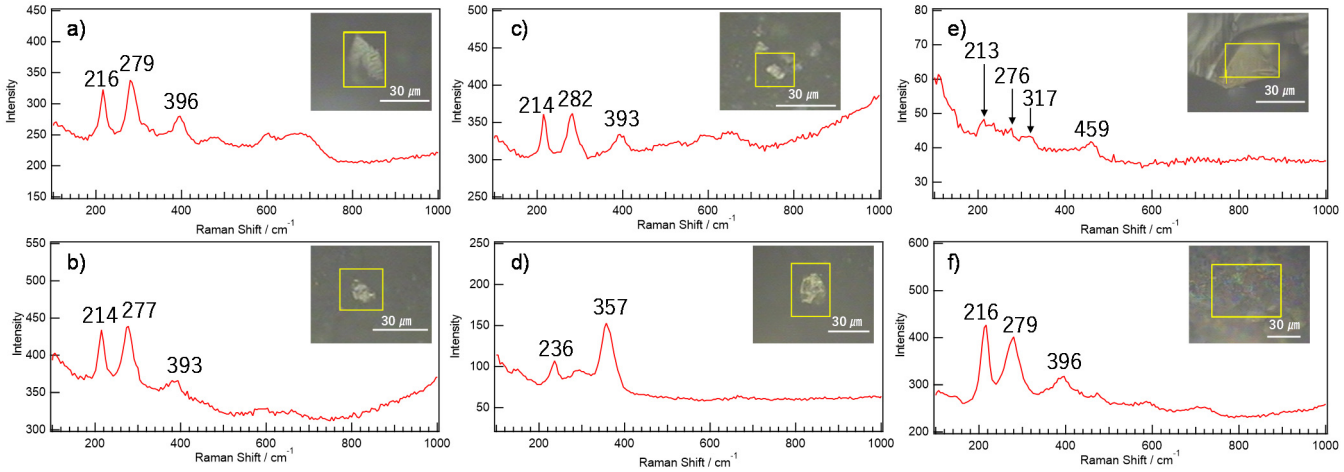

Figure 1 Raman spectra of iron sulfides on Y 980115 (a-d) and the terrestrial rocks (e: freshly cleaved surface, f: long-time air-exposed surface).

References

[1] Y. Homma et al., *J. Mineral. Petrol. Sci.*, **110**, 276 (2015) and references within.
[2] P. Lindgren et al., *Meteorit. Planet Sci.*, **48**, 1074 (2013).

Identifying Polymorphs of Serpentine with Micro-Raman Spectroscopy

Aruto Kashima[1], Shu-hei Urashima[1] and Hiroharu Yui[1]
[1]*Department of Chemistry, Graduate School of Science, Tokyo University of Science*

[Introduction] Serpentine, which is produced by aqueous alteration in meteorites and asteroids, is one of the most important water-bearing minerals.[1] While its ideal chemical formula is simply described as $Mg_3Si_2O_5(OH)_4$, it has several crystal polymorphs depending on the alteration environment such as temperature and pressure.[2,3] This suggests that these thermodynamic parameters at the aqueous alteration can be estimated from the serpentine polymorph. However, determination of the polymorph is still challenging while several researchers have tried it.[4,5] X-ray diffraction (XRD) is generally used to analyze the crystal structure, but it is not suitable for serpentine polymorphs. Serpentine crystal is generally too small for XRD, and there are no effective diffraction lines to unambiguously determine the crystal polymorphs.[6] Here, we propose a new way for the polymorph identification with micro-Raman spectroscopy. It is a non-destructive analytical method and its high spatial resolution (~1 μm) enables us to selectively analyze small chips of serpentines even in heterogeneous meteorites.

[Experimental] Microscopic Raman measurement was performed on a Raman-11i (Nanophoton) equipped with microscope of Eclipse Ti (Nikon). An objective lens of Nikon Plan Flour (40x/NA0.75 WD0.66), 532 nm or 785 nm laser with power of 7-20 mW at the sample face, and grating with 300 or 1200 grooves / mm were used. We purchased six serpentines collected from several mines (at Canada, Norway, Hungary, etc.) for the measurements and used them to explore the differences in polymorph.

[Results and Discussion] The Raman spectra observed were shown in Figure 1a. While no significant difference was found at a glance, the bands at ~390 and ~690 cm^{-1} showed subtle frequency-shift. These bands originate from stretching vibration of crosslinking Si-O-Si and bending vibration of SiO_4 units. Because SiO_4 units are an essential component of serpentine structure, these bands are observable for any polymorphs and their vibrational frequency are not affected by cation substitution. Instead, their frequency should be shifted with internal stress or bending of SiO_4 sheets, which is directly related to the polymorph structure. The frequency difference is more clearly seen in a biaxial plot of the peak frequencies for these modes (Figure 1b). While the frequency shift for each band is as small as 1-2 cm^{-1} so that they are hardly distinguishable, they are clearly separated in the biaxial plot. By macro/microscopic observation and the comparison of the spectra with those in literature, we concluded that the peak separation in the biaxial plot is owing to polymorph specificity. Assignment for each group in the biaxial plot and the detailed mechanism of the frequency shift will be described in the presentation.

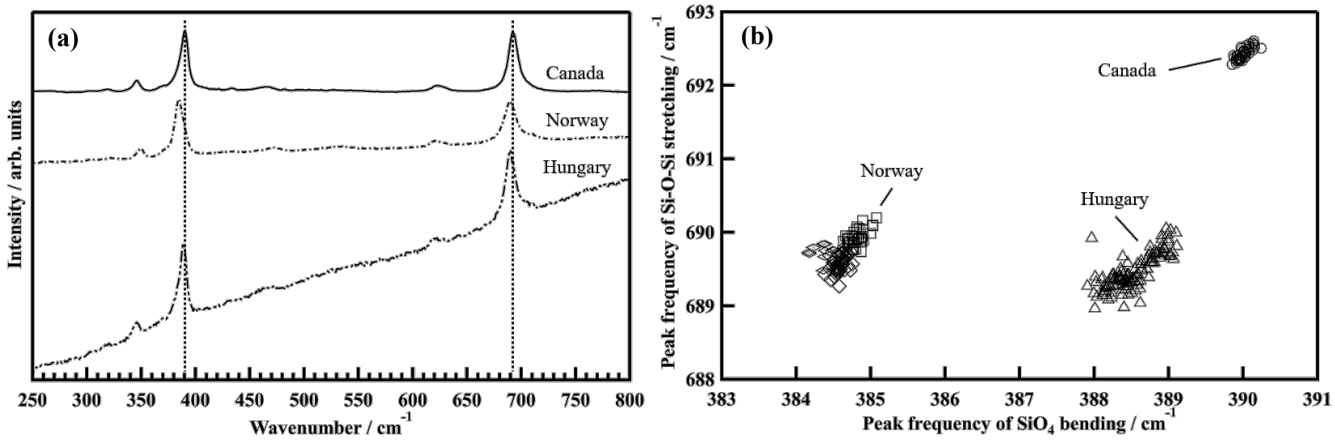

Figure 1. (a) Raman spectra of serpentine, and (b) a biaxial plot of the peak frequency

References

[1] A. J. Brearly, The Action of Water, Meteorites and the Early Solar System II, 587-624, 2006. [2] A. Putnis, An Introduction to Mineral Sciences, 2008. [3] J. J. Hemley, J. W. Montoya, C. L. Christ and P. B. Hostetler, Mineral equilibria in the MgO-SiO_2-H_2O system: talc-chrysotile-forsterite-brucite stability relations, Am. J. Sci, 277, 322-351, 1977. [4] C. Rinaudo, D, Gastaldi and E. Belluso, Characterization of chrysotile, antigorite and lizardite by FT-Raman spectroscopy, Can. Mineral., 41, 883-890, 2003. [5] I. Sakaguchi, Y. Kouketsu, K. Michibayashi and R. W. Simon, Attenuated total refrection infrared (ATR-IR) spectroscopy of antigorite, chrysotile, and lizardite, J. Mineral. Petrol. Sci., 115, 303-312, 2020. [6] N. Kohyama, Analysis of each polytype of serpentine minerals and the application to industrial health and geological science, Nendo Kagaku, 46, 33-39, 2007.

Erg Chech 002 – A New Member of the (Trachy-) Andesite Meteorite Clan

V.H. Hoffmann[1], P. Schmitt-Kopplin[2], K. Wimmer[3], M. Kaliwoda[1,4], W. Schmahl[1,4]. [1]Faculty of Geosciences, Dep. Earth and Environmental Sciences, Univ. Munich; [2]Helmholtz-Center, Munich; [3]Nördlingen; [4]Mineralogical State Collection Munich, SNSB, Germany.

In recent years, a new and unique group of meteorites was identified, and classified within the ungrouped achondrites. These meteorites are characterized by partly significantly high contents of plagioclase and/or various silica phases such as cristobalite, trydimite (or sometimes quartz) and can be placed in the fields of andesites / trachyandesites. Almahata Sitta paired individuals MS-MU 011 and MS-MU 035 were the first meteorites of this new type indicating silica-rich trachyandesitic magmatism, in this case possibly a near-crustal or upper mantle formation on the ureilite parent body [1-4].

NWA 7325/8409 and pairs ("green beauty") represent another unique set of ungrouped achondrites and was classified as a cumulate olivine-microgabbro containing more than 50% of feldspar – plagioclase - and clinopyroxene (diopside). Oxygen isotopy indicates similarities concerning formation / origin (likely parent body) to the two Almahata Sitta individuals [1-4].

NWA 11119 (and paired NWA 11558) attracted the meteorite community even further: the silica content of this stone was found to be as high as at least 30%, mainly characterized by cristobalite / trydimite and only traces of quartz. Further main phases are plagioclase – anorthite – and diopside – a fascinating whitish – green rock. Practically all phases are frequently found in small cavities in beautifully crystallized idiomorphic crystals. [1-5, and refs herein].

NWA 11575 represents another recent find in this direction, classified as an ungrouped achondrite, petrologically also a trachyandesite with an oxygen isotopy linked to the LL region. [1,2].

Erg Chech 002 was found in 2020 in the Erg Chech region of the Sahara Desert in Algeria. A number of large stones (in kg masses) and numerous smaller individuals have been found, about 32 kg in total (other sources speak about >40 kg). The unique achondrite is proposed to be a likely fragment of a chondritic protoplanet which is over 4.5 billion years old [1,2,6-10].

Methods and techniques

Here we report results of our systematic investigations by LASER Raman spectroscopy – mineralogy and phase composition. We have a number of EC 002 samples for our studies: several fragments and 2 larger pieces (slice and endcut of several grs in mass, see figure 1).

Fig 1a: A 6,7 gr endcut (left side) and (b) a 3,3 gr slice (right side) of Erg Chech are some of the samples under study in our project. Erg Chech 002 is characterized by the presence of large (green) pyroxene xenocrysts (mainly OPX) which can be recognized easily in both samples.

All Raman experiments have been performed on unprepared and uncoated samples in order to avoid any unwanted preparation effects (eg alterations). We believe that the results are really representative because we used a number of different samples. We used the 532nm LASER, Raman shifts were detected between 50-2500 cm^{-1} with a precision of +/- 1-2 cm^{-1}, and magnifications of 100-1000x (long distance lenses only), and a lateral resolution of 0.1 µm. Large maps up to 15x15 points in 2D/3D at high resolution allowed to also detect accessory phases / submicron articles and inclusions. Acquisition times of 1-3 sec and accumulation numbers of up to 5 have been used which allowed to obtain large numbers of Raman Spectra in short times within the high resolution mappings, and therefore the results should be quite representative.

The priority of this part of our project was on the major phases and their distribution / intergrowth, and the comparison with several other trachyandesitic ungrouped achondritic meteorites (MS-MU 011/035, NWA 7325/8409 and NWA 11119) which we have investigated in earlier projects [3-5].

The following phases could be found by our LASER Raman experiments in Erg Chech 002:

1. Major phases:
Orthopyroxene (OPX) (large xenocrysts)
Plagioclase / Oligoclase (partly in idiomorphic crystals in small cavities); no maskelynite.
Cristobalite / trydimite (no quartz)
Clinopyroxene (CPX) (partly in idiomorphic crystals in small cavities)

2. Accessory phases:
Troilite
Merrilite
Ca-Mg carbonates
Carbon phases (various)
Olivine-group phases (no Fe-Mg olivines, details under study)
Very few and tiny metal particles
Iron-oxides (chromite??)

Erg Chech ist characterized by a low shock degree, terrestrial alteration effects can be neglected (very low degree). A preliminary compilation of the magnetic susceptibility data which we have obtained on the above mentioned trachyandesitic ungrouped achondrites under study in our projects and Erg Chech 002 gave the following result: the Log MS value of 3,17 (log spec. magnetic susceptibility in 10^{-9} m^3/kg) of Erg Chech 002 is in the range of Log MS of MS-MU 011/035 but significantly higher as log MS of NWA 11119 and NWA 7325/8409 [4,5]. This in reasonable agreement with the concentrations of the major (ferri-o) magnetic phases in these achondritic meteorites.

References
[1] Meteoritical Bulletin Database (10/2021): Almahata Sitta, NWA 7325/8409, NWA 11119 (and pairs), Erg Chech 002.
[2] www.meteoritestudies.com: Erg Chech 002 (10/2021).
[3] T. Mikouchi, A. Takenouchi, M.E. Zolensky, V.H. Hoffmann, 2018. Almahata Sitta MS-MU-011 and MS-MU-012: formation conditions of two unusual rocks from the ureilite parent body. # 2383 and refs. herein.
[4] V.H. Hoffmann, T. Mikouchi, R. Hochleitner, M. Kaliwoda, K. Wimmer, 2018. Unique NWA 11119/11558, NWA 7325 (and pairs) and Almahata Sitta individuals MS-MU 011/035: new light on very early parent body differentiation. NASA/LPI Differentiation 2018, # 4018 and refs. herein.
[5] V.H. Hoffmann, K. Wimmer, R. Hochleitner, M. Kaliwoda, 2018. NWA 11119 – probing an unknown early planetary body? # 2468 and refs. herein.
[6] Barrat J.A., et al., 2021. A 4,565-My-old andesite from an extinct chondritic protoplanet. PNAS 118/11.
[7] Mikouchi T., Zolensky M.F., 2021. Mineralogy and cooling history of ungrouped achondrite Erg Chech 002. LPSC, #2457.
[8] Nicklas R.W., et al., 2021. Multi-stage differentiation history of andesitic achondrite Erg Chech 002. LPSC, #1074.
[9] Carpenter P.K., et al., 2021. Mineralogy and bulk elemental composition of ungrouped relatively sodic gabbroic achondrite Erg Chech 002: an ancient planetary crustal sample? LPSC, #2205.
[10] Hamann C., et al., 2021. Petrography of fine-grained domains in ungrouped achondrite Erg Chech 002: evidence for different cooling histories? 84th Meteor. Soc. Conf., #6236.

Chemical classifications of nine new iron meteorites from Yamato Mountains, Balchen and Nansen Ice field

Naoki Shirai[1], Akira Yamaguchi[2], Makiko K. Haba[3] and Shun Sekimoto[4]

[1]*Tokyo Metropolitan University,* [2]*National Institute of Polar Research,* [3]*Tokyo Institute of Technology,* [4]*Institute for Integrated Radiation and Nuclear Science, Kyoto University*

Introduction

It was announced that seven and two iron meteorites were collected from ice field near the Yamato Mountains by JARE-41, and from the Balchen and Nansen Ice Field by the Japan-Belgium joint expeditions, JARE-51 and JARE-54/BELARE 2012-2013, respectively [1]. In this report, chemical compositions of these iron meteorites were determined by using both INAA and LA-ICPMS and these chemical characteristics were discussed in detail.

Experiments

Nine iron meteorites (Y 000311, Y 000479, Y 000537, Y 000547, Y 000587, Y 000703, Y 000846, A 09179 and A 12016) were investigated in this study. All iron meteorites were analyzed by using both LA-ICPMS and INAA. INAA was performed at Institute for Integrated Radiation and Nuclear Science, Kyoto University. INAA procedure used in this study is basically similar to that reported by Shirai et al. [2]. LA-ICPMS analysis were carried out using a Thermo ElementXR coupled to CETAC LAS-213 at NIPR. Iron meteorites were ablated on line mode with spot size of 100 μm at a scan speedrate of 25-50 μm/s. All analyses were performed with 20Hz repetition rate and 100% power output. Under these conditions, ^{31}P, ^{53}Cr, ^{57}Fe, ^{59}Co, $^{60, 61, 62}$Ni, $^{63, 65}$Cu, $^{69, 71}$Ga, $^{73, 74}$Ge, ^{75}As, ^{95}Mo, $^{101, 102}$Ru, ^{103}Rh, $^{105, 106}$Pd, $^{182, 183, 184}$W, $^{185, 187}$Re, $^{189, 190}$Os, $^{191, 193}$Ir, $^{194, 195}$Pt and ^{197}Au were monitored in low resolution (R = 300). Three to five separates lines were selected by avoiding of microscopically inclusion of troilite and schreibersite and analyzed. For quantification, North Chile (IIAB), Hoba (IVB), NIST 663 are used as reference samples. Elemental abundances were determined from more than two isotopes for some elements, average values are calculated.

Results and Discussion

IID: A 09179 has chemically similar to IID. As the IID iron meteorites have a high model abundance of schreibersite, their P abundances were higher than 2400 ppm [3]. In contrast, A 09179 has a lower P abundance (800 ppm) than those of IID iron meteorites. This difference is explained by avoiding schreibersite in LA-ICPMS analysis. Among IID iron meteorites, A 09179 has lower Au abundance than those reported values for IID iron meteorites, indicating that A 09179 was early crystallized among the IID iron meteorites so far.

IIIAB: Y 000311, Y 000703 and A 12016 are plotted on the chemical trend (e.g., Au vs. Ge) defined by the IIIAB iron meteorites, suggesting that these three iron meteorites are classified into IIIAB iron meteorites. Chemical compositions for Y 000311 and Y 000703 are consistent with each other. Based on sample location and similar chemical composition, Y 000703 are paired with Y 000311. Y 790724 was classified into previously observed IIIAB iron meteorite. As Ir abundance (9.25 ppm) of Y 790724 [4] is higher than these two iron meteorites (7.36 ppm for Y 000311 and 7.27 ppm for Y 000703), these two iron meteorites are not paired with Y 790724, and it is concluded Y 000311 and Y 000703 are new members of IIIAB iron meteorites. A 12016 is the first IIIAB iron meteorite recovered from the Nansen Ice field.

IAB-ungrouped: The four iron meteorites (Y 000479, Y 000537, Y 000547 and Y 000587) analyzed in this study are plotted in the area of IAB iron meteorites in plots of Ni, Co, Ga, As and Ir vs. Au. These six elements have been used as the best taxonomic elements for classifications on IAB iron meteorite into a main group (MG) and five subgroups (sLL, sLM, sLH, sHH and sHL) [5]. Worsham et al. [6] determined highly siderophile elements (HSEs) abundances for 58 IAB iron meteorites and found that each subgroup has a characteristic CI-chondrite normalized abundance pattern for HSE. Y 000537 is plotted in the area defined by sLM except for Co. CI-chondrite normalized values for Re, Os, Ir, Ru and Pt are consistent with each other and lower than that of Pd. Y 000537 has a similar Pd abundance to those for sLM subgroups, while its CI-chondrite normalized abundances patterns for HSE are different from those of sLM and similar to those for sHL and sHH subgroups. The observed pattern of Y 000537 is broadly similar to magmatic iron meteorites such as IIAB and IIIAB, indicating that Y 000537 was fractionally crystallized. Three Yamato iron meteorites (Y 000479, Y 000547 and Y 000587) have similar chemical compositions to each other, implying that Y 000547 and Y 000587 are paired with Y 000479. These three iron meteorites are not plotted in the area defined by any IAB subgroups. CI-chondrite normalized abundance patterns for HSE of

these three iron meteorites are similar to those for sHL and sHH subgroups. Thus, the four Yamato iron meteorites (Y 000479, Y 000537, Y 000547 and Y 000587) are classified into IAB-ungrouped.

References

[1] Meteorite Newsletter (2020) vol. 27. [2] Shirai N. et al. (2015) JRNC 303:1375-1380. [3] Buchwald V. F. (1975) Handbook of Iron Meteorites. Univ. California Press. [4] Wasson J. T. and Kallemeyn G. W. (2002) GCA 66:2445-2473. [5] Worsham E. A. et al. (2016) GCA 188:261-283. [6] Wasson J. T. et al. (1989) GCA 53:735-744.